

## Distribution Agreement

In presenting this thesis or dissertation as a partial fulfillment of the requirements for an advanced degree from Emory University, I hereby grant to Emory University and its agents the non-exclusive license to archive, make accessible, and display my thesis or dissertation in whole or in part in all forms of media, now or hereafter known, including display on the world wide web. I understand that I may select some access restrictions as part of the online submission of this thesis or dissertation. I retain all ownership rights to the copyright of the thesis or dissertation. I also retain the right to use in future works (such as articles or books) all or part of this thesis or dissertation.

Signature:

---

Arshad Karumbamkandathil

---

Date

**Fluorescence Quenching in single CdSe/CdS Dot-In-Rod Nanostructures using  
Modified Atomic Force Microscopy tips**

By

Arshad Karumbamkandathil  
Master of Science

Chemistry

---

Dr. Tianquan Lian  
Advisor

---

Dr. Francesco Evangelista  
Committee Member

---

Dr. Susanna Widicus Weaver  
Committee Member

Accepted:

---

Lisa A. Tedesco, Ph.D.  
Dean of the James T. Laney School of Graduate Studies

---

Date

**Fluorescence Quenching in single CdSe/CdS Dot-In-Rod Nanostructures using  
Modified Atomic Force Microscopy tips**

By

Arshad Karumbamkandathil

BS-MS Dual Degree, Indian Institute of Science Education and Research (IISER)

Bhopal, 2013

Advisor: Tianquan Lian, PhD

An Abstract of  
A thesis submitted to the Faculty of the  
James T. Laney School of Graduate School of Emory University  
in partial fulfillment of the requirements for the degree of  
Master of Science  
in Chemistry  
2016

## Abstract

Fluorescence Quenching in single CdSe/CdS Dot-In-Rod Nanostructures using Modified Atomic Force Microscopy tips

By Arshad Karumbamkandathil

The main objective of this thesis is to study the quenching of fluorescence in single CdSe/CdS dot-in-rod (DIR) nanostructures via electron transfer (ET) using modified AFM tips. AFM tips were either modified with TiO<sub>2</sub> nanoparticles (NP), or commercially available Pt AFM tips were used for this study. Electron Transfer from DIR to TiO<sub>2</sub> or Pt was shown, by measuring the quenching in photoluminescence (PL) intensities and lifetimes of single CdSe/CdS DIRs.

It was seen that the fluorescence quenching is uniform along the length of the DIR, suggesting the ET process from DIR to TiO<sub>2</sub> NP or Pt is the rate-determining step and dominates over ionization, diffusion, and recombination rates. Cross-section dependent study showed that quenching occurs only within the tip radius in contact with the DIR and is dependent on the tip material and geometry. Vertical tip-DIR separation study showed that the quenching can occur only when the tip is in close contact with the DIR. Control experiments with regular Si AFM tips showed that quenching can occur only when an electron acceptor like TiO<sub>2</sub> or Pt is attached to the AFM tip, suggesting charge transfer to be occurring.

**Fluorescence Quenching in single CdSe/CdS Dot-In-Rod Nanostructures using  
Modified Atomic Force Microscopy tips**

By

Arshad Karumbankandathil

BS-MS Dual Degree, Indian Institute of Science Education and Research (IISER)

Bhopal, 2013

Advisor: Tianquan Lian, PhD

A thesis submitted to the Faculty of the  
James T. Laney School of Graduate Studies of Emory University  
in partial fulfillment of the requirements for the degree of  
Master of Science  
in Chemistry  
2016

## Table of Contents

Chapter 1 Introduction .....	1
1.1 Theory of Fluorescence.....	1
1.2 Fluorescence Lifetime and Quantum Yield.....	3
1.3 Semiconductor Nanoparticles .....	4
1.4 From bulk CdSe to quantum confined nanocrystals.....	5
1.5 Relaxation process in Semiconductor Nanocrystals: Non-radiative and radiative transitions .....	7
1.5.1 Non-radiative relaxations.....	7
1.5.2 Radiative relaxation or Fluorescence.....	9
1.6 Core/Shell Nanocrystals.....	11
1.7 CdSe/CdS dot-in-rods.....	13
1.8 CdSe/CdS DIRs coupled with metal nanocrystals.....	15
1.9 Fluorescence Quenching.....	16
Chapter 2 Experimental Setup and Sample Preparation .....	20
2.1 Synthesis of CdSe/CdS DIRs: .....	20
2.2 Synthesis of TiO <sub>2</sub> Nanoparticles:.....	20
2.3 Atomic Force Microscopy (AFM) and Tip Functionalization (single TiO <sub>2</sub> NP attachment to an AFM Tip):.....	21
2.4 Single Molecule Fluorescence Spectroscopy.....	22
2.5 Time-Correlated Single Photon Counting (TCSPC) Technique.....	24
2.6 Fluorescence Intensity and Lifetime Measurements.....	25
2.7 Fluorescence Intermittency or Blinking.....	26

2.8 Using Single Molecule Fluorescence to study interfacial ET.....	29
Chapter 3 Results and Discussion.....	32
Summary and Future Outlook.....	41
References .....	42

## Chapter 1. Introduction

### 1.1 Theory of Fluorescence:

Luminescence can be regarded as the emission of light from any molecule and occurs typically from electronically excited states. The source of excitation is absorption of photons, which promotes the molecule into an electronically excited state. Depending on the nature of the excited state, i.e. whether the emission is occurring from a triplet excited state ( $T_1$ ) or a singlet excited state ( $S_{1,2}$ ) to a singlet ground state ( $S_0$ ), luminescence can be categorized as Phosphorescence and Fluorescence respectively. Phosphorescent emission rates are in the order of  $10^3$  to  $1\text{ s}^{-1}$ , whereas fluorescent emission occurs at much faster time scales in the order of  $10^8$  to  $10^9\text{ s}^{-1}$ .

After light absorption, a molecule is excited to a higher excited state, which can then undergo several processes to reach the ground state ( $S_0$ ): internal conversion and intersystem crossing with no emission; phosphorescence and fluorescence with emission of photons. This can be clearly visualized by using a Jablonski diagram<sup>1</sup> as shown in Figure 1. The singlet ground, first and second electronic states are depicted by  $S_0$ ,  $S_1$  and  $S_2$ , respectively. The triplet electronically excited state is denoted as  $T_1$ . At each of these electronic states, the molecules can exist in a number of vibrational energy levels, depicted by 0, 1, 2, etc. The transitions between states are shown as vertical lines, with solid and dotted lines representing radiative (absorbing or emitting photons) and non-radiative processes, respectively.

Absorption and emission occur mostly from molecules with the lowest vibrational energy. The energy difference between the singlet ground and excited states is too large for thermal population of  $S_1$ . For this reason, light is used instead of heat to induce

fluorescence. A molecule is usually excited to a higher vibrational level of either  $S_1$  or  $S_2$ . The molecules then rapidly relax to the lowest vibrational level of  $S_1$ . This process is known as internal conversion and typically occurs within  $10^{-12}$  s. Since fluorescence lifetimes are near  $10^{-8}$  s, internal conversion is completed prior to emission. Hence fluorescence results from the lowest vibrational state of  $S_1$ . Molecules in the singlet  $S_1$  state can also undergo a spin conversion to the triplet  $T_1$  state, this process is called intersystem crossing. Emission from  $T_1$  is known as phosphorescence, transitions from  $T_1$  to  $S_0$  is spin-forbidden, as a result, the rate constants for phosphorescence are several orders of magnitude smaller than those for fluorescence.<sup>1</sup>

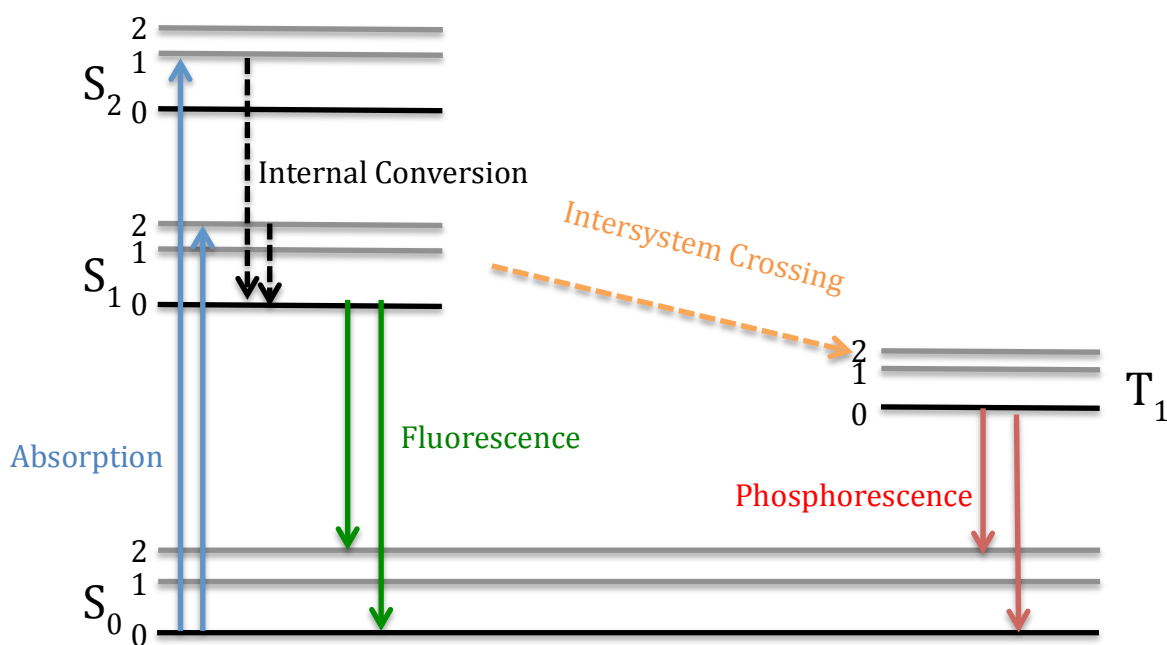


**Figure 1. The Jablonski Diagram. Singlet ground, first and second electronic states are labeled as  $S_0$ ,  $S_1$  and  $S_2$ , respectively. Triplet state is labeled as  $T_1$ . 0, 1 and 2 are the vibrational states of each electronic state. Various processes following light absorption, namely internal conversion, intersystem crossing, fluorescence and phosphorescence are also shown.**

## 1.2 Fluorescence Lifetime and Quantum Yield

Fluorescence Lifetime and Quantum Yield (QY) are usually the most important characteristics of a fluorescent molecule (fluorophore). QY can be simply defined as the number of emitted photons per number of absorbed photons. Fluorescence lifetime and QY can be best understood with the aid of a simplified Jablonski diagram (Figure 2). This diagram focuses only on those processes, responsible for the return to ground state  $S_0$  (individual relaxation processes leading to the relaxed  $S_1$  state have been excluded). In particular, this diagram focuses on the emissive rate of the fluorophore ( $k_r$ ) and its non-radiative decay rate ( $k_{nr}$ ) to  $S_0$ .

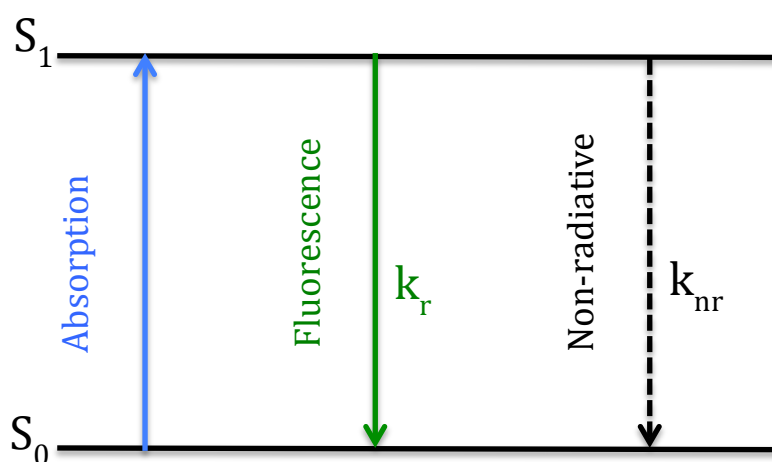


**Figure 2. A simplified Jablonski diagram showing fluorescence and non-radiative decay rates from  $S_1$  to  $S_0$  after light absorption.**

Both  $k_r$  and  $k_{nr}$  depopulate the excited  $S_1$  state. The fraction of fluorophores that decay through emission, and hence the quantum yield, is given by

$$QY = \frac{k_r}{k_r + k_{nr}} \quad (1)$$

Fluorescence lifetime can be defined as the time a fluorophore spends in the excited state before returning to the ground state, by emitting a photon.

$$\tau = \frac{1}{k_r + k_{nr}} \quad (2)$$

The lifetime of the fluorophore in the absence of non-radiative processes is called the intrinsic or natural lifetime ( $\tau_n$ )

$$\tau_n = \frac{1}{k_r} \quad (3)$$

$$\tau_n = \frac{\tau}{QY} \quad (4)$$

### 1.3 Semiconductor Nanocrystals

Semiconductor nanomaterials have attracted a great deal of interest in recent years owing to their unique characteristics and promising applications ranging from biological dynamics<sup>2,3</sup> and biomolecular imaging<sup>4-6</sup> to light emitting diodes (LEDs),<sup>7-9</sup> solar cells<sup>10</sup> and interfacial charge transfer dynamics.<sup>11-15</sup> They possess unique properties because of their size-tunability and high intrinsic photoluminescence (PL) quantum yields (QYs).<sup>16,17</sup> Reducing the size to the nanometer scale and tuning the shape of the semiconductor can change its electronic and optical properties dramatically when compared to the bulk material. Synthesis of nanometer size crystals in solution resulting in the formation of colloidal nanocrystals has increased tremendously in recent years and has a wide range of applications. Colloidal nanocrystals synthesized today are known to be fluorophores with high photostabilities at room temperature. Photostability of nanocrystals is particularly important in experiments where photobleaching is a limiting factor for imaging and light emitting applications.<sup>18-20</sup>

Among colloidal nanocrystals, Cadmium Selenide (CdSe) is one of the most studied nanomaterials owing to its easy and high quality synthesis. By tuning their size, one can have different CdSe nanocrystals with emission covering almost the entire visible

spectrum. Several pioneering studies on single spherical CdSe nanoparticles revealed the emission properties hidden by previous ensemble measurements, such as fluorescence intermittency (blinking) or spectral diffusion.<sup>16,21</sup> Reducing these effects has been an intense topic of research in order to obtain fluorescent nanoparticles with a steady emission rate and emission spectra.

With the advent of new synthetic techniques and methods, the above-mentioned drawbacks have been progressively overcome. First, CdSe nanocrystals were coated or capped by a thin spherical layer of another semiconductor material, Zinc Sulfide (ZnS), to form semiconductor heterostructures, increasing the photoluminescence QY.<sup>22,23</sup> Later on, capping with thicker shells of Cadmium Sulfide (CdS) considerably enhanced the average emission rate by reducing the blinking or fluorescence intermittency, when compared to bare CdSe nanocrystals.<sup>24</sup> Synthesis of elongated particles with a cylindrical shape, called nanorods, paved the way to control the shape of colloidal nanocrystals. For our study, we are primarily concerned with a specific type of CdSe/CdS heterostructure called dot-in-rods (DIRs),<sup>25-27</sup> which are composed of a CdSe spherical core (seed) embedded in a cylindrical rod-like CdS shell (discussed later).

#### **1.4 From bulk CdSe to quantum confined nanocrystals**

Quantum confinement<sup>28,29</sup> means that if the size of the semiconductor nanocrystal becomes closer to or smaller than the De Broglie wavelength of the charge carriers (electrons and holes) for this specific material, then the charges are confined inside the material. The confinement changes dramatically the energy states of the carriers. The

energy spectrum then shifts from a continuum of allowed states for the bulk material to an atomic like behavior as the bulk energy levels become quantized.

CdSe is a direct band-gap semiconductor (same k-vector). Dispersion relations,  $E(k)$  for the conduction band (CB) and valence band (VB) of bulk CdSe having a minima and maxima, respectively at  $k = 0$  can be approximated as

$$E_{CB} = \frac{\hbar k^2}{2m_e^*} + E_g \quad (5)$$

$$E_{VB} = \frac{\hbar k^2}{2m_h^*} \quad (6)$$

where,  $m_e^*$  and  $m_h^*$  are the effective masses of free electrons and holes, respectively, and  $E_g$  is the band gap of the material.

After absorption of a photon, an exciton: electron-hole pair bound primarily by Coulombic interaction is created and can be described as a hydrogen-like atom. A Bohr radius for this exciton can be written as

$$r_B = \epsilon \frac{m_0}{\mu} r_0 \quad (7)$$

where,  $r_0$ : the Bohr radius of the hydrogen atom,  $\epsilon$ : dielectric constant of the material,  $m_0$ : electron rest mass, and  $\mu$ : reduced mass of the electron-hole pair.

By comparing the nanocrystal radius ( $a$ ) and the exciton Bohr radius ( $r_B$ ), two regimes of quantum confinement can be defined: (1) a weak confinement regime ( $r_B < a$ ), which is typically the case for self-assembled or bulk CdSe and, (2) a strong confinement regime ( $r_B > a$ ), as seen in CdSe nanocrystals. According to the Bloch's theorem, the electron and hole wave functions in a bulk nanocrystal can be defined as

$$\psi_{nk}(r) = e^{ikr} u_{nk}(r) \quad (8)$$

where,  $u_{nk}(r)$  is a function of the crystal lattice periodicity,  $k$  is the wave vector

associated to the particle and  $n$  is the band index associated to a given band (conduction band or valence band). Inside a nanocrystal, an electron or a hole wave function in a given band can be written as a linear combination of Bloch functions,

$$\psi_{nk}(\mathbf{r}) = \sum_k C_{nk} e^{i\mathbf{k}\cdot\mathbf{r}} u_{nk}(\mathbf{r}) \quad (8)$$

with  $C_{nk}$  satisfying the boundary conditions of the infinite potential well problem.

## **1.5 Relaxation process in Semiconductor Nanocrystals: Non-radiative and radiative transitions**

### **1.5.1 Non-radiative relaxations**

We now look at the various relaxation processes that take place inside CdSe nanocrystals. After excitation above the band gap, one or more excitons are created in the continuum of the energy states that will first relax non-radiatively through lattice interactions and carrier scatterings. Thus, for a given electronic state of the nanocrystal, the probability that a photon will be emitted is always less than unity.

### **Interactions with phonons**

Interactions of the carriers (electrons and holes) with the ion lattice takes place during the relaxation of the carriers in their respective bands, this is called intraband relaxations. This interaction is also important to understand the band-edge relaxation of an exciton, this relaxation can excite one or more phonons.

### **Auger processes**

The process of energy transfer between carriers via Coulomb interactions is an Auger process. It happens between two carriers or more. In CdSe nanocrystals for which the strong confinement regime applies, even though the Coulombic potential is

considered as a perturbation and the accessible energy levels are quantized, Auger processes are strongly enhanced. We now look at different Auger mechanisms and their consequences on CdSe nanocrystals photoluminescence.

**Electron thermalization:** This Auger process occurs between two carriers, where the electron relaxes towards the band edge giving its energy to the hole. The holes can relax by successive emission of phonons.<sup>30</sup>

**Multiexciton relaxations:** Auger relaxations of multiple excitons can also take place in CdSe nanocrystals. It involves at least three charge carriers, where the non-radiative recombination of an electron-hole pair takes place, and transfers its energy to a third carrier, an electron or a hole as shown in Figure 3.

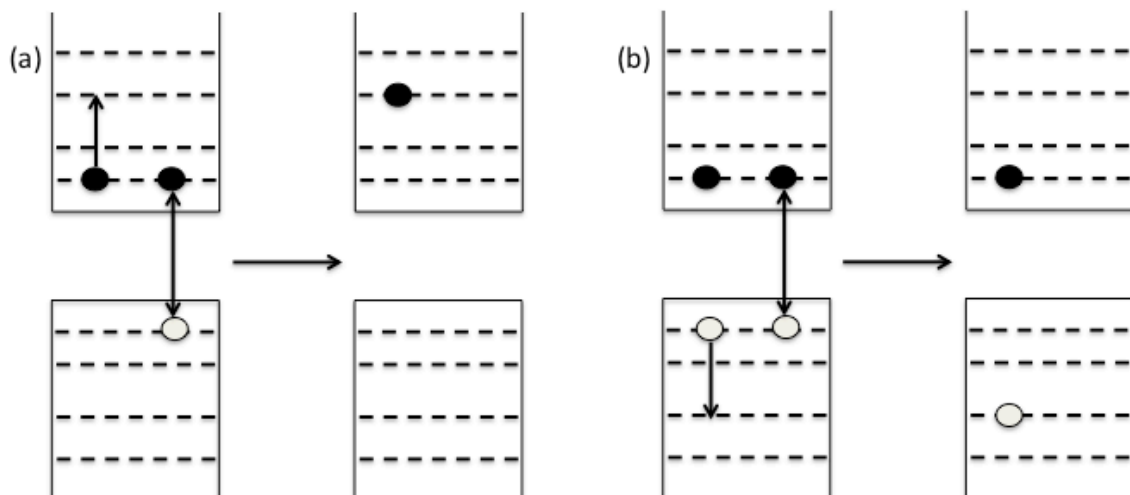


**Figure 3. Auger recombinations. a) Auger process involving the decay of a ground state trion b) Auger process involving the decay of a ground state biexciton**

First, the nonradiative relaxation of a trion (an electron-hole pair plus an extra charge: a charged exciton) through an Auger energy transfer is depicted in Figure 3a: the extra charge is promoted to a higher energy state after taking the recombination energy of

the electron-hole pair. This process is very efficient in bare CdSe nanocrystals.<sup>16</sup> Since the first observation of emission intermittency (blinking) from single particle fluorescence measurements,<sup>31</sup> the random switching between ON emission periods where photons are detected and OFF periods where the nanocrystal is not emissive has been attributed to the charging of the nanocrystals. The trion emission is quenched by the Auger relaxation mechanism. The second important case that is described in Figure 3b involves the nonradiative recombination of a biexciton. One electron-hole pair gives its recombination energy to one charge of a neighboring electron-hole pair. This mechanism prevents the photon emission from multiple excitons and explains the single photon emission of CdSe nanocrystals observed at room temperature.<sup>32-34</sup>

### 1.5.2 Radiative relaxation or Fluorescence

The origin of semiconductor nanocrystal fluorescence comes from the radiative recombination of electron-hole pairs, which are generated by a photon absorption process. Semiconductor nanoparticles, in general, have full valence band (VB) and an empty conduction band (CB), due to quantum confinement. After excitation, an electron is excited from a VB to a CB, leaving behind a hole in the VB. The electron and hole can then recombine by fluorescence emission.

Let us now consider the single exciton Hamiltonian. An electron is photogenerated to the CB from the VB, leaving a hole in the VB, to form an exciton. The corresponding Hamiltonian of the exciton has the form

$$H_0 = -\frac{\hbar^2 \nabla_e^2}{2m_e^*} - \frac{\hbar^2 \nabla_h^2}{2m_h^*} - \frac{e^2}{4\pi\epsilon|r_e - r_h|} + V_c(r_e) + V_v(r_h) \quad (9)$$

where,  $m_e^*$  and  $m_h^*$  are effective masses of the electron and hole, respectively. The

confinement potential is in the form of

$$V_n(\mathbf{r}) = \begin{cases} -\Delta_n, & b \leq 1 \\ 0, & \text{otherwise} \end{cases} \quad (10)$$

where,  $n=c$  for CB electrons and  $n=v$  for VB holes,  $b = (x^2 + y^2 + z^2)/a^2$ ,  $a$  is the radius of the nanocrystal.  $\Delta_n$  is the CB offset between the nanocrystal and the surrounding medium. The eigen solution of equation (9) is denoted as exciton state  $j$ ,

$$H_0(\mathbf{r}_e, \mathbf{r}_h) \psi_j(\mathbf{r}_e, \mathbf{r}_h) = E_j \psi_j(\mathbf{r}_e, \mathbf{r}_h) \quad (11)$$

Denoting  $\mathbf{A}$  as the vector potential of the electromagnetic field, the Hamiltonian describing the electromagnetic interaction is  $V = e\mathbf{A} \cdot \mathbf{p}/m_0$ . The wave function of the total system composed of electrons and photons is

$$\Psi(\mathbf{r}, t) = \sum_j C_j(t) \psi_j(\mathbf{r}) \exp(-iE_j t/\hbar) |N_{\hbar\omega}\rangle \quad (12)$$

where,  $|N_{\hbar\omega}\rangle$  describes the photon field with  $N$  number of photons. The following equation is obtained for the wave function coefficient,

$$i\hbar \frac{dC_j(t)}{dt} = \frac{e}{m_0} \sqrt{\frac{\hbar}{2\omega\epsilon\Omega}} \sum_i \langle \psi_j(\mathbf{r}) | a \cdot \mathbf{p} | \psi_i(\mathbf{r}) \rangle C_i(t) \left\{ \sqrt{N_{\hbar\omega}} \exp\left[\frac{i(E_j - E_i - \hbar\omega)t}{\hbar}\right] + \sqrt{N_{\hbar\omega} + 1} \exp\left[\frac{i(E_j - E_i - \hbar\omega)t}{\hbar}\right] \right\} \quad (13)$$

by inserting Eq. 12 into the time-dependent Schrodinger equation. The headed by  $\sqrt{N_{\hbar\omega}}$  corresponds to the photon absorption, while the one with  $\sqrt{N_{\hbar\omega} + 1}$  is the photon emission.  $N_{\hbar\omega}/\Omega$  is the photon density.

Multiple electron-hole pairs (X) can also be created inside a nanocrystal at high excitation power. A radiative relaxation is characterized by its radiative decay rate also known as the rate of spontaneous emission. The rate of emission depends on two factors: the light emitter with its intrinsic properties and the density of electromagnetic modes of

the emitter-surrounding medium.

## **1.6 Core/Shell Nanocrystals**

The capping of CdSe nanocrystals by another material like CdS has attracted a lot of interests in recent years.<sup>35,36 37</sup> The optical properties can drastically change when capping bare CdSe nanocrystals with various materials of different shapes and sizes. In general, the addition of a shell greatly enhances the efficiency of emission. The nanocrystal surface is passivated by the ligands adsorbed during the synthesis. However, the ligands do not passivate the whole nanocrystal surface. Many dangling bonds are close to the nanocrystal core; they act as nonradiative decay channels and quench the photoluminescence. Fluorescence quantum yield in core-only nanocrystals is usually less than 10%. Moreover, capped nanocrystals exhibit a better photostability than bare CdSe.

### **Classification of core/shell heterostructures**

Capping of the core with a specific shell can impact the carrier's wave function. A particle will be strongly confined in the core if the capping material has a band gap well above the core band gap. When decreasing the band gap difference between the two materials, the carriers start to expand more and more inside the shell. This can potentially result in a change of radiative rate if the overlap decreases. Depending on the capping material and its band alignment compared to the core, we can classify the core/shell heterostructures as shown in Figure 4.

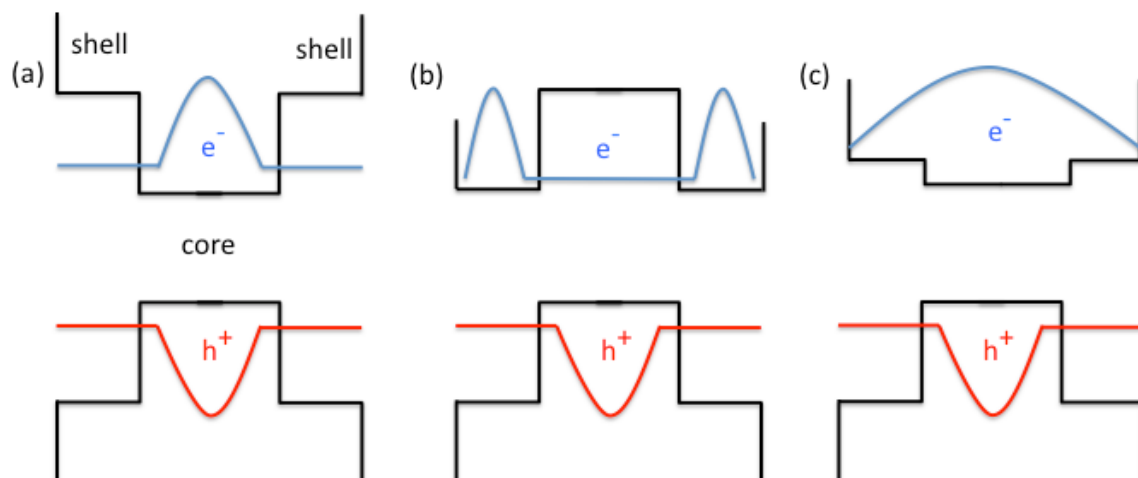


**Figure 4. Classification of core/shell heterocrystals: (a) Type I (b) Type II (c) Quasi Type II heterostructures. Blue and red lines are the wave functions of the electrons and the holes, respectively.**

Type I heterostructures depicted in Figure 4a, the shell is used to passivate the surface of the core with the goal to improve its optical properties. The shell physically separates the surface of the optically active core from its surrounding medium. In comparison to bare nanocrystals, core/shell heterostructures exhibit generally enhanced stability against photobleaching and photodegradation. At the same time, the shell growth reduces the number of surface dangling bonds, which can act as trap states of charge carriers and thereby reduce the fluorescence QY. They have a band alignment such that both the valence and conduction bands of the core material are located within the energy gap of the shell. In this case, both electrons and holes wave functions are mostly localized inside the core. The typical type I nanocrystal is CdSe/ZnS, where carriers wave functions are strongly localized within the core.<sup>22</sup> The ZnS shell significantly improves the fluorescence QY and stability against photobleaching.<sup>22,38</sup>

Type II heterostructures depicted in Figure 4b have their lowest energy states for

electrons and holes with the corresponding wave functions localized in different materials. The energy gradient at the interfaces tends to spatially separate electrons and holes on different sides of the heterojunction. The growth of the shell induces a strong redshift of the spectrum as carriers are spatially separated. Also, the lifetime of the emission considerably increases because of the small carrier wave functions overlap.<sup>38</sup> Typical heterostructures showing Type II behavior include CdTe/CdSe, CdSe/ZnTe and ZnSe/CdS.<sup>39,40</sup> Type II heterostructures have been developed in particular for emission in the near-infrared wavelengths,<sup>41</sup> lasing<sup>42</sup> because of their reduced Auger effects, photovoltaics applications<sup>40</sup> because of the possibility to collect the separated charges before any recombination.

Finally, heterostructures for which the carrier wave functions are only partially overlapping are called Quasi Type II heterostructures. This is the case if one of the bands shows only a slight offset between the two materials as shown in Figure 4c. In this case, one of the charges is well confined inside one material while the other is delocalized over the whole structure. CdSe/CdS is the typical example of Quasi Type II heterostructure. The electron is delocalized inside the entire structure. The hole is confined inside the core due to the large valence band offset.<sup>43-47</sup>

### **1.7 CdSe/CdS dot-in-rods**

In the previous sections, we have discussed the principal ideas about bare CdSe nanocrystals and the effects of adding a capping layer of a given semiconductor material around it. With this knowledge, we now look at CdSe/CdS dot-in-rods (DIRs) made of a spherical CdSe core embedded inside a rod-like shell (Figure 5), synthesized using the

seeded growth approach developed by Carbone et al.<sup>27</sup> Typical absorption and emission spectra from an ensemble of dot-in-rods in solution are also shown in Figure 5.

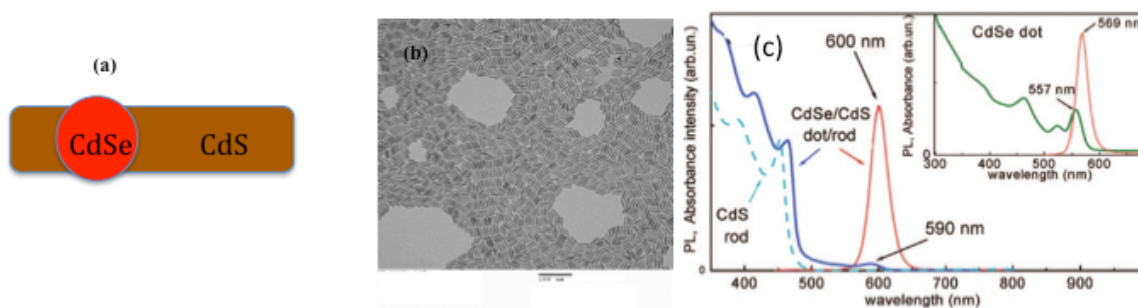


**Figure 5. (a) Schematic diagram of the CdSe/CdS DIR. (b) TEM image. These DIRs have a length of 109 ( $\pm 1.0$ ) nm and a diameter of 3.6 ( $\pm 0.3$ ) nm. (c) Absorption and emission spectra of dot-in-rods. Absorption (blue line) and emission spectra (red line) of CdSe/CdS DIR. Dashed blue line is the absorption of a CdS rod. Inset: Absorption and photoluminescence of only CdSe core.**

The dark blue line is the absorption spectra of CdSe/CdS DIR; it is very similar to the absorption curve (dashed, light blue line) of CdS rods only. The very steep absorption onset below 500 nm is characteristic of CdS absorption. The CdS shell with its rod shape and large material amount dominates the absorption curve of DIRs. In the inset, we show the absorption and emission of bare CdSe seeds used in this synthesis. The absorption peak at lower energy (590 nm) of the CdSe/CdS sample can be associated with the first electronic transition of the CdSe seeds as it is not present in the CdS nanorods. It is red-shifted with respect to the corresponding transition in the seed (557 nm) due to the lower confinement induced by the shell. One major difference with bare CdSe dots or CdSe/ZnS core/shell structures is the fact that Auger recombination can be drastically reduced in CdSe/CdS heterostructures.<sup>48</sup>

## 1.8 CdSe/CdS DIRs coupled with metal nanocrystals

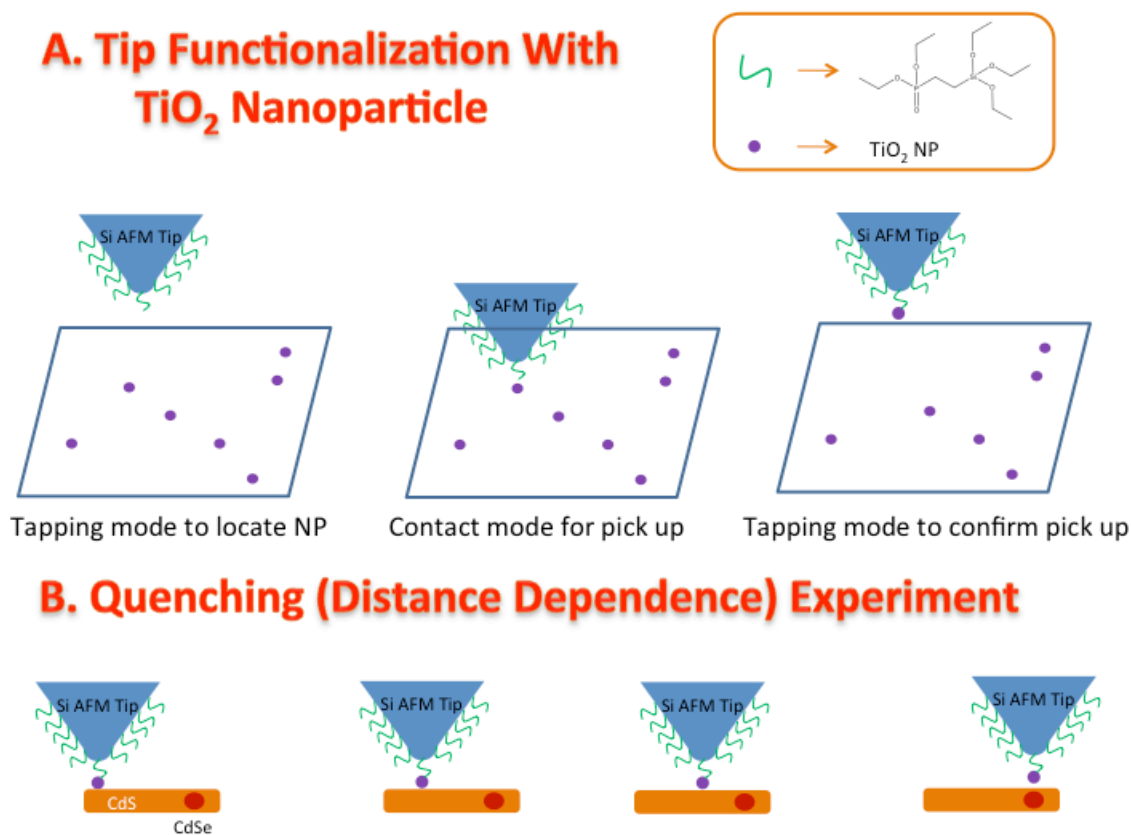
Banin and co-workers reported for the first time the synthesis of a new family of semiconductor/metal hetero-nanorods (NRs). With the help of the high reactivity of NR tips, Au nanoparticles were successfully deposited on CdSe NRs by room-temperature reduction of Au(III) salts.<sup>49</sup> These hybrid NRs combine the properties of semiconducting CdSe NRs and plasmonic Au nanoparticles, which has been demonstrated to have promising applications in solar energy conversion.<sup>50,51</sup> In particular, plasmon-induced hot electron transfer from photo-excited metal to semiconductor offers a new paradigm for light harvesting and charge separation.<sup>51,52</sup>

The most important type of hybrid NRs for solar-to-fuel conversion is perhaps the Pt tipped NRs, because Pt is considered as one of the best catalysts for hydrogen evolution reaction.<sup>53</sup> These NRs, combining the light harvesting capability of CdS and catalytic activity of metal domains, have been intensely studied for solar driven H<sub>2</sub> generation reactions.<sup>54-59</sup> NRs have been used as light harvesting and charge separating materials to drive photoreduction reactions, including the reduction of H<sup>+</sup> to generate H<sub>2</sub>.<sup>60</sup> The quantum efficiency of these light driven reactions depends on the rate of interfacial electron and hole transfer from NRs and the competing charge recombination processes. Thus, efficient photocatalysis requires control of these charge transfer and recombination rates through tailoring the NR morphology and composition. Due to quantum confinement in the radial directions in NRs, ultrafast interfacial charge transfer can be expected to occur. The large surface area of NRs allows adsorption of more charge acceptors, which should enhance charge transfer rates because of the additive nature of charge transfer channel. Fast carrier transport along the long axis suggests the possibility

of long distance charge separation.<sup>60</sup>

## 1.9 Fluorescence Quenching

Fluorescence quenching refers to any process that decreases the fluorescence intensity of the sample in consideration. A wide range of molecular interactions can result in quenching. These include electron transfer, energy transfer, proton transfer, excited state reactions, molecular rearrangements, excimer formation and collisional quenching.<sup>1</sup> The main objective of this thesis is to look at the fluorescence quenching induced by the interaction of Atomic Force Microscopy (AFM) tips, which modifies the fluorophore's



Scheme 1. (A) AFM tip functionalization, Si AFM tip modified (using a bifunctional linker, shown in the top right corner) with a single TiO<sub>2</sub> nanoparticle. First, tapping mode is used to locate the TiO<sub>2</sub> nanoparticles, followed by contact mode to attach a

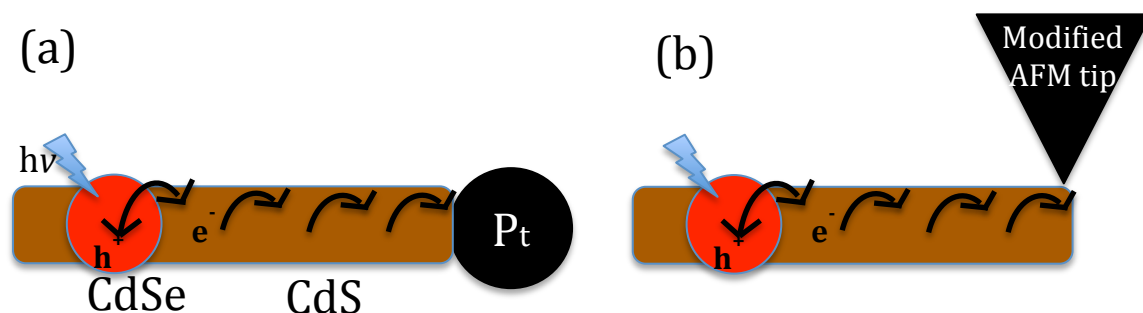
**single TiO<sub>2</sub> nanoparticle to the tip. Finally, ortho scanning in tapping mode is done to confirm the functionalization. (B) Typical quenching experiment using the modified AFM tip on a single CdSe/CdS DIR at various distances along the length of the DIR.**

emission intensity, resulting in significant changes in the emission rates and lifetimes. This quenching effect induced by the tip mainly depends on the tip material and geometry, excitation and emission wavelength, the particle quantum yield, and most importantly the distance between the tip and the emitter.<sup>61,62</sup> Regular AFM tips (Si tip material) can be modified to attach a single TiO<sub>2</sub> nanoparticle which can act as a quencher for these studies (Scheme 1). Alternatively, commercially available Pt AFM tips can also be used to see this effect.

In Pt tipped CdSe/CdS DIRs, the VB hole can be localized to the CdSe core.<sup>56,63</sup> The charge separation efficiency in these DIRs was shown to be near unity and charge separated states are long-lived for both excitation at the CdSe seed and the CdS rod.<sup>57</sup> Considering the long distance, typically 10s of nm, between electron donor (CdSe core) and acceptor (Pt tip) in these hetero-NRs, efficient ET cannot occur through tunneling mechanism.<sup>64</sup> A possible mechanism is the thermally-activated electron hopping (Scheme 2a) in which the electron is first dissociated from the hole by thermal activation and then diffuses along the CdS rod to reach the Pt tip.<sup>65-67</sup>

The work of this thesis, tries to mimic the CdSe/CdS-Pt tipped DIR system, such that we use a modified AFM tip (TiO<sub>2</sub> and Pt) to look at the ET from the DIR to the tip. The main objective of this study to see how the emission properties of the DIR can be controlled, modified and optimized by an adjacent nanostructure, like TiO<sub>2</sub> and Pt, and to

see this quenching effect by the modified tip at different distances along the DIR. Yoskovitz et al<sup>68</sup> had recently shown that emission was mainly quenched at a sub-20 nm of the CdSe/CdS DIR heterostructure using distance-dependent lifetime imaging and examining the tip-particle distance-dependent interaction in tapping AFM mode. In contrast, we observed that this quenching in fluorescence intensity and emission lifetime is uniform along the length of the DIR (Scheme 1) in contact mode (see experimental details section). We attribute this quenching effect arising from electron transfer from the DIR to the TiO<sub>2</sub> nanoparticle or the Pt AFM tip, rather than energy transfer through dipole-dipole interaction that was reported earlier. Doing a control experiment, using regular Si AFM tips, where no quenching was seen, further supported this. Contact mode would give us a better picture to understand this phenomenon, since the tip is always in contact with the DIR, whereas in tapping mode the tip is oscillating and electron transfer cannot always take place.



**Scheme 2. Schematic diagram of a possible mechanism for the long-range electron transfer in (a) CdSe/CdS–Pt DIR and (b) CdSe/CdS DIR in contact with a modified AFM tip, which involves thermal dissociation of electron from hole and random hopping of electron along the rod to reach the metal nanostructure**

This work focuses on the ET dynamics from single DIRs to TiO<sub>2</sub> modified and Pt AFM tips. It was found that the ET from DIR to TiO<sub>2</sub> or Pt AFM tips takes place

uniformly along the length of the DIR, irrespective of the core location. Previous studies<sup>68</sup> however showed that energy transfer is the predominant mechanism through which fluorescence quenching occurs, and was localized to take place in the seed location. This discrepancy can be explained, only if, the ET to TiO<sub>2</sub> or Pt is the rate-determining step, i.e., electrons can diffuse along the length of the DIR, by thermally-activated electron hopping process<sup>69-71</sup> (Scheme 2b) in a faster time scale than the ET process. This would also explain the uniformity in the ET along the DIR. More systematic studies are needed to test the validity of this model. A control experiment with unmodified Si AFM tip was done, and no quenching or energy transfer was observed.

## Chapter 2. Experimental Setup and Methods

### 2.1 Synthesis of CdSe/CdS DIRs:

DIRs used in this study were synthesized by a seeded-growth procedure.<sup>61,69,70</sup> CdS (with its first excitonic peak at 380 nm) and CdSe quantum dots (with its first excitonic peak at 500 nm) were used as the seed for rod growth. Typically, 0.06 g Cadmium Oxide (CdO), 3 g Trioctylphosphine oxide (TOPO), 0.29 g Octadecylphosphonic acid (ODPA), and 0.08 g hexylphosphonic acid (HPA) were degassed under vacuum for ~ 1 hour at 150<sup>0</sup>C. After heating to 350<sup>0</sup>C under nitrogen for half an hour, the CdO was dissolved and the mixture turned clear. At this point, 1.8 ml Trioctylphosphine (TOP) was injected. In a separated container, sulfur injection solution (0.12g S in 1.8 mL TOP) was mixed with CdS or CdSe QDs. The amount of seeds in a typical synthesis was  $8 \times 10^{-8}$  mol. When the temperature of the Cd-containing solution was stabilized at 350<sup>0</sup>C, the seed-containing Sulfur injection solution was swiftly injected. The solution was allowed to react for 8 min. Products were precipitated out of the reaction crudes by addition of ethanol. The precipitation processes were repeated for several times. Finally DIRs were dispersed in hexane. To prepare samples for single molecule study, a DIR solution with concentration of ~ 10 pM was spin-coated directly on glass coverslips.

### 2.2 Synthesis of TiO<sub>2</sub> Nanoparticles:

TiO<sub>2</sub> colloidal nanoparticles and thin films were prepared by following reported methods.<sup>71</sup> Briefly, TiO<sub>2</sub> colloid nanoparticles were prepared by hydrolysis of titanium(IV) isopropoxide in a mixture of glacial acetic acid and water at 0<sup>0</sup>C. The

colloid was concentrated at 80°C, autoclaved at 230°C for 12 h, and then stirred for 4 days.

### **2.3 Atomic Force Microscopy (AFM) and Tip Functionalization (single TiO<sub>2</sub> NP attachment to an AFM Tip):**

Si AFM tip from MikroMasch, USA was used. Briefly, the tip was immersed in a solution of (2-Diethylphosphatoethyl) triethoxysilane (purchased from Gelest, Inc) for a period of 1 hour. The main purpose of using this bifunctional linker was to attach the silane moiety to the AFM tip such that the phosphate moiety can be used to pick up a TiO<sub>2</sub> NP (spin coated on pre cleaned glass coverslip). The modified tip was then used to scan TiO<sub>2</sub> NPs (tapping mode, Figure 6a) and locate the positions of NPs. Once the position of the single TiO<sub>2</sub> NP is known, contact mode was used to attach the NP to the AFM tip. This attachment was confirmed by scanning the same area using tapping mode, as the NP cannot be seen in the AFM image (Figure 6b).

All measurements were done at room temperature and ambient conditions. Briefly an AFM head (Asylum Research MFP-3D-BIO) was mounted on the inverted microscope (described earlier). For correlated AFM topography and fluorescence measurements, the AFM tip was positioned within the diffraction-limited excitation spot. Using a piezo-electric mirror the excitation spot was changed finely such that the AFM tip is perfectly aligned to the excitation spot. The AFM images were recorded by tapping (AC) mode with the tip-sample distance (z) oscillating around an average value of 10-100 nm and the sample ortho-scanned in the x and y directions by the AFM piezo-stage. At the same time, the resulting epifluorescence was detected. Once the DIRs were located,

contact mode was used to approach the tip to the DIR to do the quenching study at different locations on the DIR.

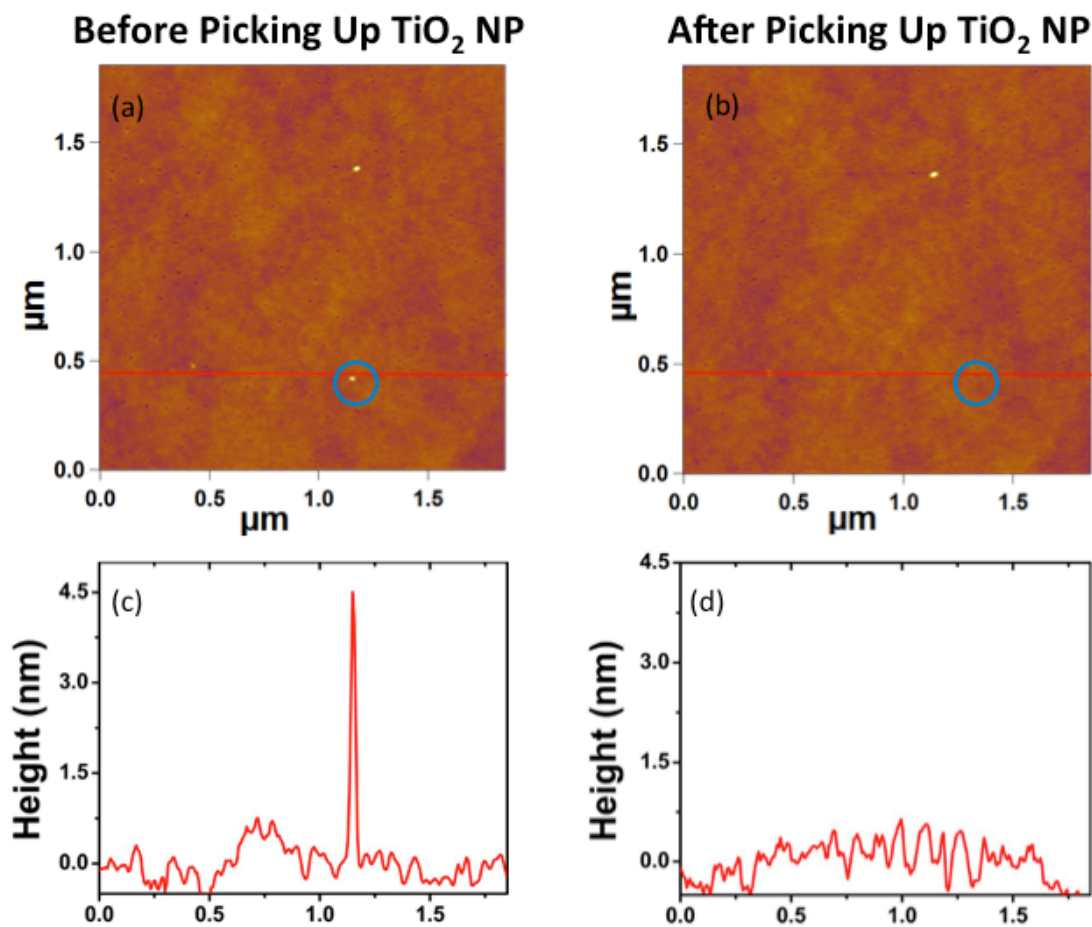


**Figure 6.** (a) and (b) are the ortho scanned AFM images of single DIRs on a glass coverslip before and after pick up, respectively. (c) and (d) are the height cross sections along the red lines in (a) and (b) respectively.

## 2.4 Single Molecule Fluorescence Spectroscopy

Single-molecule fluorescence spectroscopy has been considered as an important spectroscopic tool for quite some time now.<sup>72,73</sup> The advantages of single-molecule detection are many, apart from the fascination of looking at individual molecules at work,

single-molecule techniques can provide detailed mechanisms of photophysical processes and time-dependent pathways of chemical reactions that are hidden or impossible to synchronize at the ensemble level.

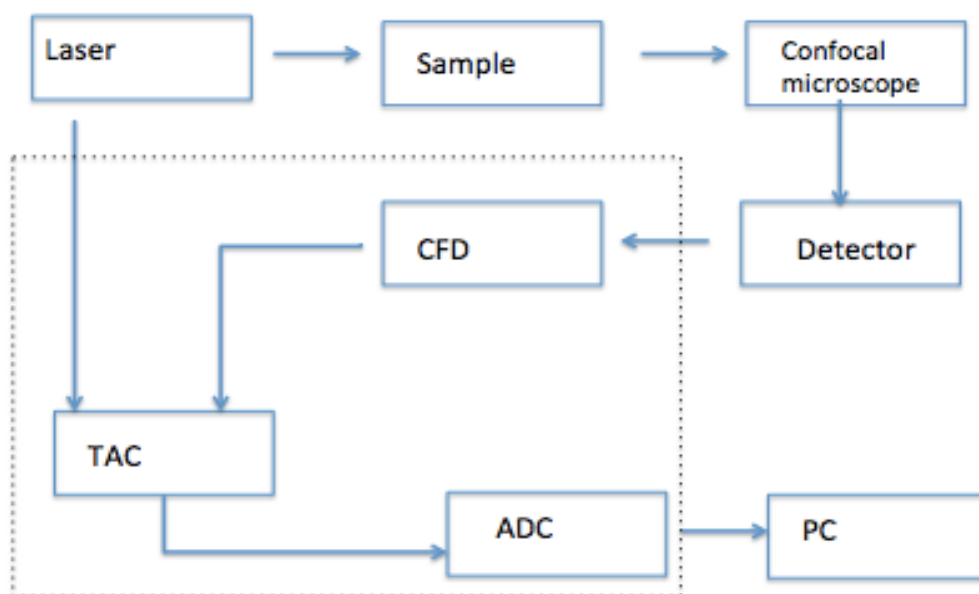
Single-molecule fluorescence measurements are typically carried out using a scanning confocal microscope. A laser pulse of an appropriate wavelength ( $\lambda$ ) is focused to a diffraction limited ( $\lambda/2$ ) spot on the sample surface through the confocal microscope in order to excite the sample. The resulting epifluorescence is collected by the microscope and detected by appropriate detectors. Chromophores with large absorption cross-sections and high fluorescence quantum yields are preferred in order to maximize the signal-to-noise ratio. If the molecules on the sample surface are located far enough away from each other (the average distance between molecules should be  $> \lambda/2$ ), only one molecule is photoexcited at a time, and the fluorescence from only that single molecule is collected. Plots of fluorescence intensity as a function of time (fluorescence intensity trajectories) can then be obtained, revealing dynamics on the millisecond (ms) to second (s) time scale. Furthermore, when using pulsed lasers and time-correlated single photon counting (TCSPC), fluorescence lifetime trajectories can be gathered, revealing the dynamics on the hundreds of picoseconds (ps) to nanoseconds (ns) time scale.

Interfacial electron transfer (ET) processes can lead to changes in single molecule fluorescence intensities that can be detected and analyzed. The interfacial ET mechanism and dynamics at the nanoscale play a vital role in surface chemistry, catalysis and solar energy conversion. Hence understanding the kinetic rate processes and dynamics that govern the interfacial ET is of crucial importance.<sup>13,31,74-80</sup>

## 2.5 Time-Correlated Single Photon Counting (TCSPC) Technique

Photon counting is an intensity measurement technique based on the quantum nature of light. TCSPC technique (Scheme 3) detects and counts individual photons from the signal. The advantages of single photon counting (SPC) over traditional analog method of measurements are:

- (i) SPC is insensitive to the drift and noise associated with the instrument.
- (ii) Digital nature of SPC simplifies both the acquisition as well as analysis of the data.

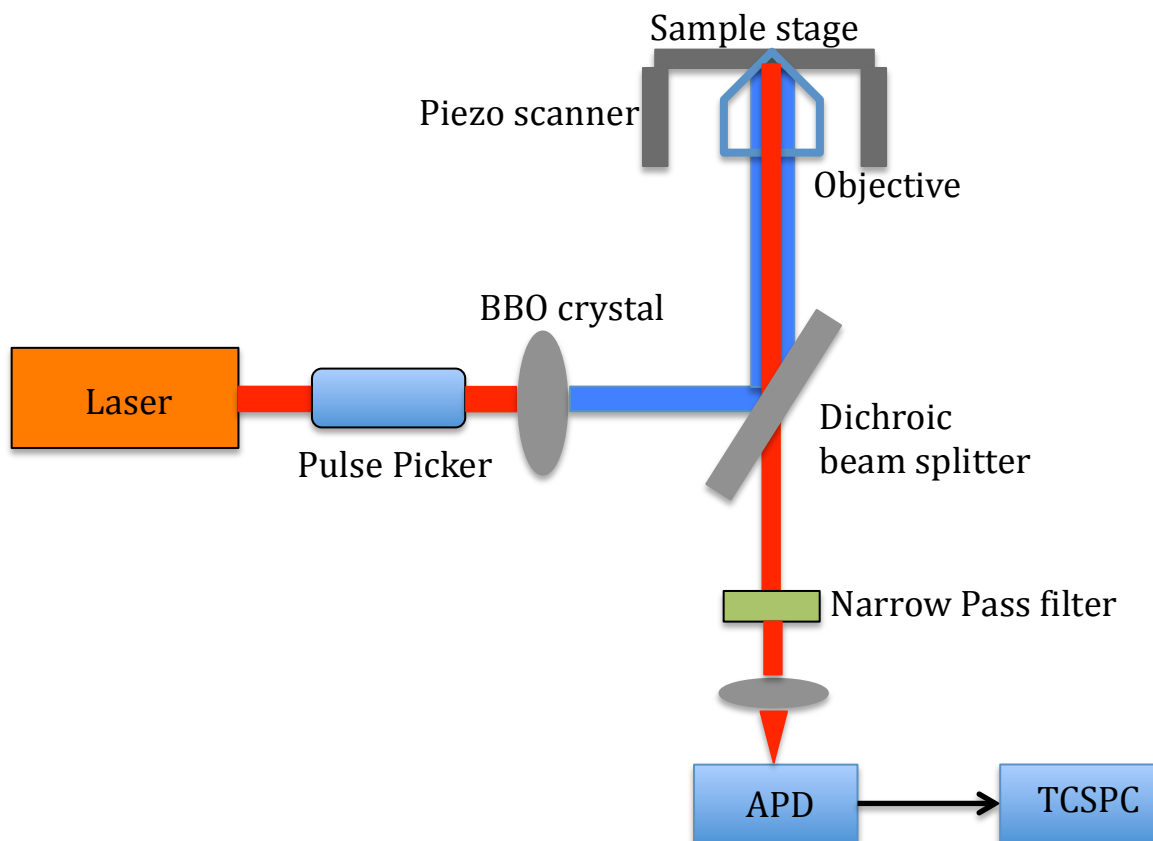


**Scheme 3. Schematic block diagram of a typical TCSPC Setup**

Time resolution in single molecule spectroscopy is also desirable in many fundamental studies: to investigate the charge transfer dynamics from single QD/DIR to adjacent charge acceptors<sup>15,68,81,82</sup>. By integrating a confocal microscope with time-resolved techniques, such as TCSPC, time resolved single molecule spectroscopy can be used to study the fluorescence dynamics on a single particle level.

## 2.6 Fluorescence Intensity and Lifetime Measurements

Single DIR fluorescence detection was carried out with an optical scanning confocal microscope (Scheme 4). Femtosecond laser pulses ( $\sim 100$  fs) with a repetition rate of 80 MHz were generated with a mode-locked Ti:Sapphire laser (Tsunami oscillator pumped by 10 W Millennia Pro, Spectra-Physics).



**Scheme 4. Schematic diagram of the confocal microscope setup coupled with TCSPC.**

The output centered at 980 nm was passed through a pulse picker (Conoptics, USA) to reduce the repetition rate by a factor of 9, and then frequency doubled in a BBO crystal to generate 490 nm excitation pulses. The glass coverslips containing DIR were placed on a piezo scanner. The excitation beam ( $\sim 150$  nW) was focused through an

objective (100X, N.A 1.4, oil immersion, Olympus) down to a diffraction-limited spot on the sample. The resulting epifluorescence from the sample was detected by an avalanche photodiode (APD, Perkin-Elmer SPCM-AQR-14). The APD output was analyzed by a time correlated single photon counting (TCSPC) board (Becker&Hickel SPC 600). The instrument response function for the fluorescence lifetime measurement had a full width at half-maximum of  $\sim 500$  ps.

## **2.7 Fluorescence Intermittency or Blinking**

Fluorescence intermittency or blinking has been observed for various types of single nanoscale emitters,<sup>83</sup> including molecular dyes, fluorescent proteins, small nanodiamonds<sup>84</sup> and colloidal nanocrystals.<sup>16,17,85-87</sup> In colloidal nanocrystals, a broad distribution of blinking rates is observed, resulting in periods of high fluorescence (ON state) and low fluorescence (OFF state at the noise emission level) spanning from hundreds of microseconds to hundreds of seconds as seen in Figure 7. Since the first report of fluorescence blinking in small spherical nanocrystals,<sup>16</sup> this behavior has been observed for many morphologies including elongated nanorods and nanowires.

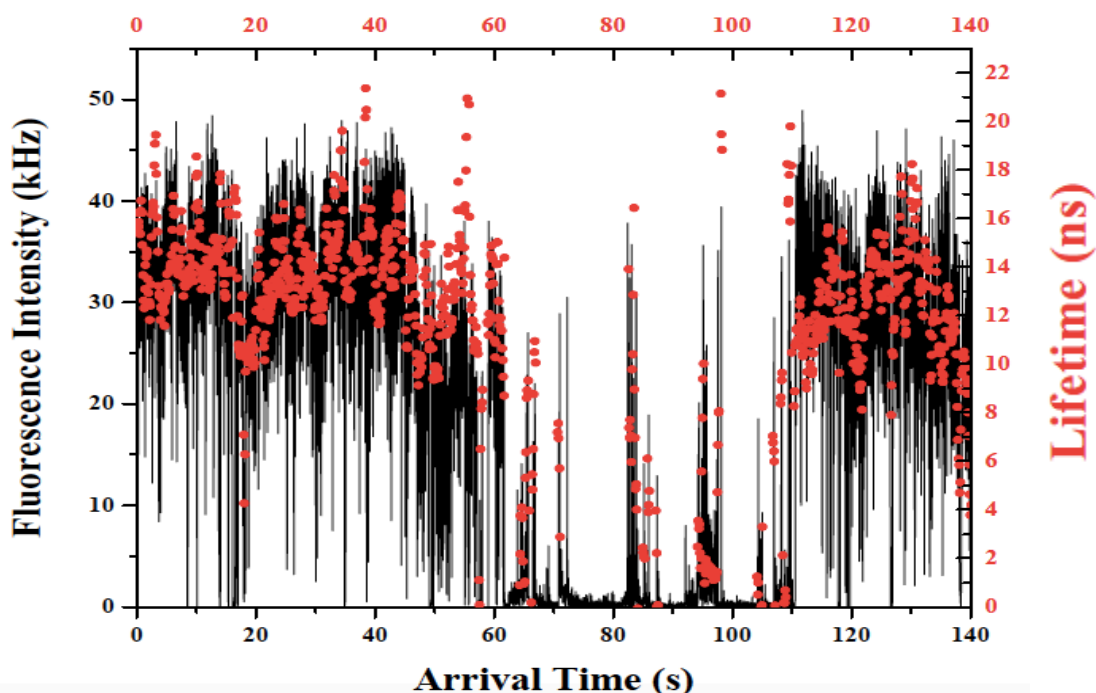


**Figure 7. Typical fluorescence intensity (black) and lifetime (red) trajectories of a single CdSe/CdS DIR on a glass coverslip.**

A prominent property of semiconductor nanocrystals is their fluorescence intermittence or blinking.<sup>16,17,73,87-93</sup> This phenomenon is buried in ensemble fluorescence detection and can only be probed by using single particle measurements. This blinking activity is attributed to the photoinduced charging of the nanocrystal through the transfer of an electron to the trap states in and around the nanocrystal.<sup>16,17,58,71-77</sup> The ON state is neutral and the exciton recombines through a radiative decay pathway, while in the OFF state it is positively charged with an electron in the trap state and a hole in the nanocrystal. Under photoexcitation, the exciton recombines through nonradiative fast Auger relaxation, quenching the fluorescence.<sup>16,21,28</sup>

One way to study the blinking is to look at the distributions of ON and OFF event durations  $P_{\text{on}}(t_{\text{on}}=t)$  and  $P_{\text{off}}(t_{\text{off}}=t)$  respectively, or at the cumulative distributions  $P_{\text{on}}(t_{\text{on}}>t)$  and  $P_{\text{off}}(\tau_{\text{off}}>t)$ . The cumulative distributions tell us the probability of the

emission to be ON or OFF for a time period longer than a duration  $t$ . A non-exponential distribution (power law distribution) was found,

$$P(t) \sim t^{-\alpha}; 1 < \alpha < 2 \quad (14)$$

To compute the distributions of ON and OFF event durations, first, the photoluminescence time trace is built from the measured photon detection events as in Figure 7 with a certain bin time. Then thresholds to discriminate between the time trace ON and OFF events need to be defined. Determining the duration of each ON and OFF events yields the cumulative distributions.

Fluorescence blinking is a direct result of charge carrier trapping. Two types of model coexist in the literature to link the charge trapping with the non-fluorescent periods observed during blinking:

**Type A blinking:** This model assumes that the charge trapping of one type of carrier leaves the nanocrystal core charged by the unpaired remaining carrier.<sup>94</sup> It is also known as the charging/discharging model. The Auger recombination being an efficient non-radiative recombination pathway in nanocrystals, the unpaired charge in the core induces a low fluorescence quantum yield because most of the electron-hole pairs recombine non radiatively with the extra charge by Auger effect. The low fluorescence lasts for a time dictated by the lifetime of the trapped charge. Once the trapped charge recombines with its countercharge, the low fluorescence period is over. The ON emission state is a succession of absorption and radiative recombination of charges. An ON to OFF switching occurs via thermal ionization, tunneling or Auger-assisted photo-ionization<sup>93</sup> of a charge carrier to a trap state. The trapped charge leaves a charge of opposite sign inside the nanocrystal. The resulting charged nanocrystal remains non fluorescent, despite the

subsequent absorption cycles, because of the fast non radiative Auger energy transfer. The OFF to ON switching occurs when the trapped charge returns into the nanocrystal and recombine with its countercharge.

**Type B blinking:** This model states that the trapped charge recombines non radiatively with its countercharge promptly after each excitation event and therefore there is not a permanent charging of the core during low fluorescence periods. The low fluorescence periods correspond to fast charge trapping rates that dominate radiative recombination rate. Intermittency is caused by time-dependent fluctuations of that trapping rate. When the charge trapping rate becomes much slower than the radiative rate, the nanocrystal is in a ON fluorescence period. The durations of the OFF state are dictated by the time scales of the trapping rate fluctuations and not by the lifetime of the trap state as in the type A model. An ON period occurs when the trapping rate is considerably slower than the fluorescence rate, after absorption, an exciton is created and recombines radiatively. The switching from the ON to the OFF state occurs when the trapping rate becomes much faster than the fluorescence rate. During an OFF period the nanocrystal cycles between photon absorption to create an exciton, fast removal of the charge to a trap state, and non radiative recombination of the electron and trapped hole. OFF to ON switching occurs when the trapping rate becomes very slow again. This can be due to fluctuations of the distribution of trap states on the surface. The blinking of semiconductor nanocrystals can be affected by the interfacial ET, such that in presence of ET we can clearly see a decrease in the number of ON states and hence enhancement in blinking.

## **2.8 Using Single Molecule Fluorescence to study interfacial ET**

Photoinduced interfacial electron transfer (ET) is a widely studied process due to

its applications in solar cells, photocatalysis and molecular electronics. The studies on this topic have recently become more intense due to the increasing demand for environmentally clean solar energy sources. Motivated by the desire to understand and optimize the performance of solar conversion devices, the interfacial ET dynamics between molecules, QDs and semiconductor oxides have been extensively investigated.<sup>68,82,95</sup> In most previous studies, the ET dynamics were measured on the ensemble-averaged level. The interfacial ET dynamics can also be probed by time-resolved fluorescence spectroscopy. The intrinsic fluorescence decay rate ( $k_0$ ) of chromophores can be represented by the following equation:

$$\frac{1}{\tau} = k_r + k_{nr} = k_0 \quad (15)$$

where  $\tau$  is the observed fluorescence lifetime and  $k_r$  and  $k_{nr}$  are the radiative and nonradiative decay rates, respectively. In an active ET state, the fluorescence lifetimes can be shortened as follows:

$$\frac{1}{\tau'} = k_r + k_{nr} + k_{et} = k_0 + k_{et} \quad (16)$$

where  $k_{et}$  is the interfacial ET rate. The ET dynamics can then be resolved by comparing the lifetimes with and without ET.

Previous ensemble-averaged measurements have revealed multi-exponential ET dynamics for numerous systems,<sup>96-98</sup> suggesting a distribution of ET rates which transient absorption and ensemble fluorescence techniques cannot distinguish. However, single-molecule fluorescence spectroscopy has demonstrated the capability to examine the hidden static and dynamic heterogeneities in interfacial ET processes.<sup>13-16,72,73</sup> The study of interfacial ET from single molecules or particles explores how the behavior of molecules and particles may differ between each other at different times, how the

molecules are affected by their local environments, and how their ET dynamics can affect or be affected by their fluorescence properties. Single molecule fluorescence spectroscopy thus reveals the details in the interfacial ET dynamics that are obscured by ensemble averaging.

### Chapter 3. Results and Discussion

The first exciton peak of CdSe/CdS DIRs used in this study is at 400 nm (CdS) and 540 nm (CdSe). These DIRs are found to show a Quasi Type-II alignment, such that holes are confined to the CdSe core and the electrons can delocalize along the direction of the CdS rod.<sup>99</sup> The PL ensemble lifetime was found to be  $16.5 (\pm 0.3)$  ns and was fitted single exponentially (Figure 8). The excitation wavelength was 490 nm.

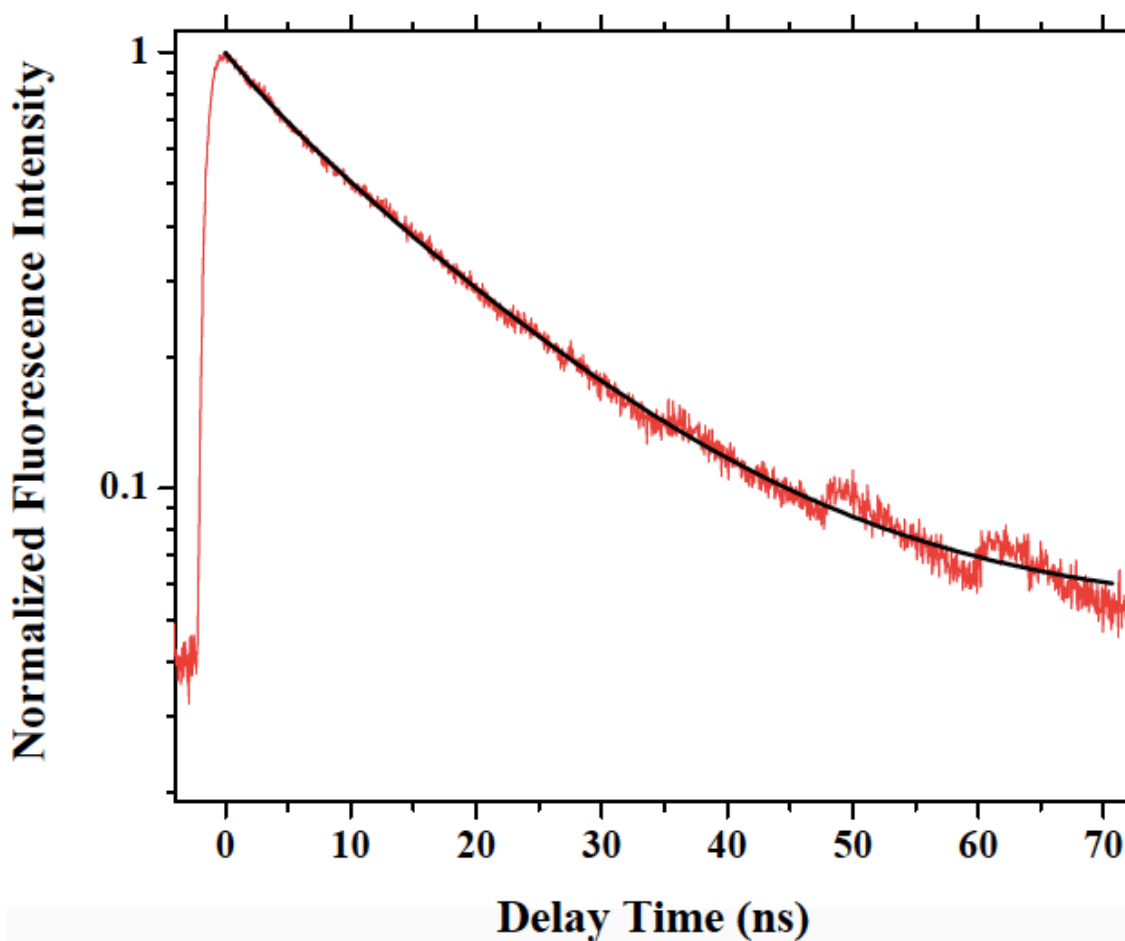


**Figure 8. Ensemble PL (red) lifetime was found to be  $16.5 \pm 0.3$  ns (black: single exponential fitted curve)**

In both single DIR and ensemble measurements, DIR fluorescence between 540 nm and 675 nm was selected using a band-pass emission filter for detection. The

collected photons were labeled by their arrival time (w.r.t the start of the experiments) and delay time (w.r.t the excitation pulse). The number of photons binned over a 50 ms window of arrival time was calculated to construct trajectories of fluorescence intensity (in units of counts per second or Hz) as a function of (arrival) time. Delay time histograms of detected photons within a 0.5 s window were constructed and fitted by single exponential decays to determine their fluorescence lifetimes. Typical fluorescence intensity and lifetime trajectories of a single CdSe/CdS DIR on a glass coverslip are shown in Figure 9(a). The corresponding histograms of fluorescence intensity and PL lifetime are shown in panels b and c in Figure 9, respectively.

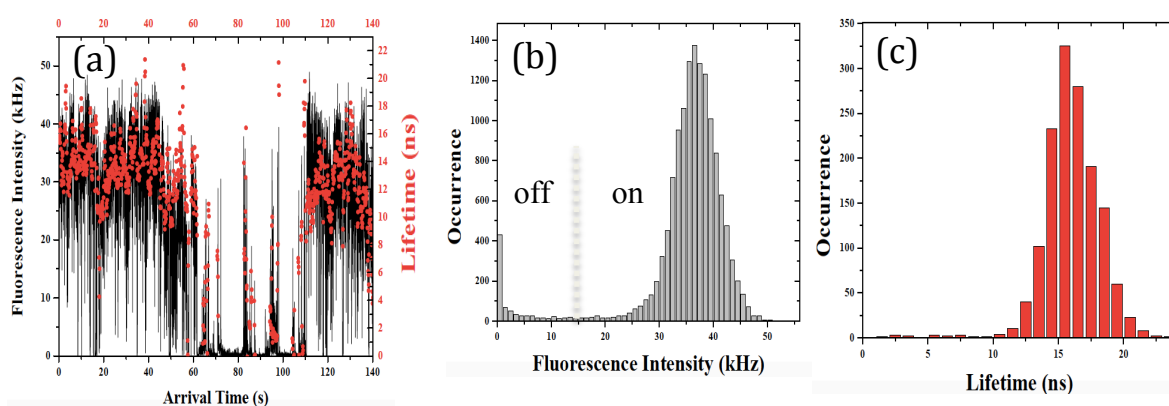


**Figure 9. (a) Typical fluorescence intensity (black) and lifetime (red) trajectories of CdSe/CdS DIR on a glass coverslip. The corresponding fluorescence intensity histograms are shown in b and c. Dashed line in b indicates the threshold separating the on and off states.**

Similar fluorescence intensity distributions have been observed for all DIRs examined. The high-intensity peak has been referred to DIRs in the on state and the low-intensity peak to those in the off state, although there was a broad distribution of intensity levels within these states.<sup>15-19</sup> To determine the threshold intensity that separates these states, the distribution was fit by a sum of two Gaussian functions. The point where these

two Gaussians cross was taken as the threshold intensity. Any point in the trajectory with intensity above (or below) the threshold level was assigned to ON (or OFF) state. The lifetimes at trajectory points with fluorescence intensity near the background level (OFF states) could not be accurately determined due to limited number of photons and were assumed to be  $< 0.5$  ns on the basis of the positive correlation.

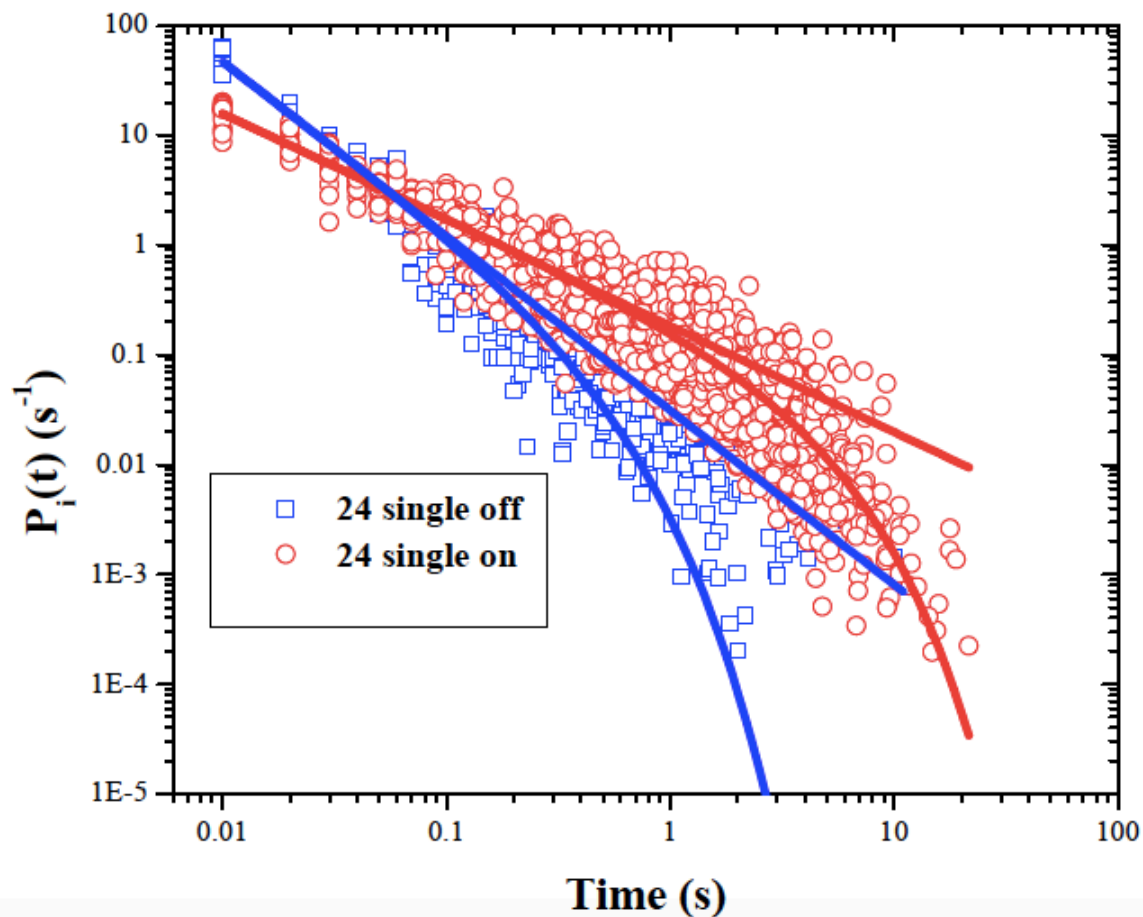


**Figure 10. Probability density of ON states ( $P_{\text{on}}(t)$ , red circles) and OFF states ( $P_{\text{off}}(t)$ , blue squares) constructed from 24 single DIRs on glass. The solid lines are best fits to equations 17 and 18.**

The probability densities  $P(t)$  of a DIR at ON or OFF states for a duration time of  $t$  are defined as

$$P_i(t) = \frac{N_i(t)}{N_{i,\text{total}}} \times \frac{1}{\Delta t_{\text{avg}}}, \quad i = \text{on or off} \quad (17)$$

where,  $N(t)$  is the number of ON or OFF events of duration time of  $t$ ,  $N_{\text{total}}$  the total number of ON or OFF events, and  $\Delta t_{\text{avg}}$  is the average time between nearest neighbor events.

As shown in Figure 10, both  $P_{\text{on}}(t)$  and  $P_{\text{off}}(t)$  of single DIRs on glass show a power law distribution at short time but deviate from this distribution at long time tails, similar to those reported by other groups.<sup>87,100</sup> These  $P(t)$  distributions can be fit by a truncated power law:<sup>100,101</sup>

$$P_i(t) = B_i t^{-m_i} \exp(-\Gamma_i t), \quad i = \text{on or off} \quad (18)$$

where,  $B$  is the amplitude,  $m$  the power law exponent, and  $\Gamma$  the saturation rate.

Next, we look at how single particle measurements were done to observe the interaction of a modified AFM with the DIR. Figure 11, panel A and panel B shows fluorescence intensity trajectories (black and red) of free DIR and quenched DIR (after contact with  $\text{TiO}_2$ ) respectively at one location on the DIR. Also shown, are intensity and lifetime histograms of the same, and thus the quenching in fluorescence intensities and lifetimes can be clearly seen. The quenching rate by electron transfer ( $K_{\text{ET}}$ ), can be expressed as

$$K_{\text{ET}} = 1/\tau_{\text{DIR-TiO}_2} - 1/\tau_{\text{DIR}} = 1/\tau_{\text{ET}} \quad (19)$$

$K_{\text{ET}}$  for this particular DIR- $\text{TiO}_2$  quenching interaction was found to be  $0.02 \text{ ns}^{-1}$ .

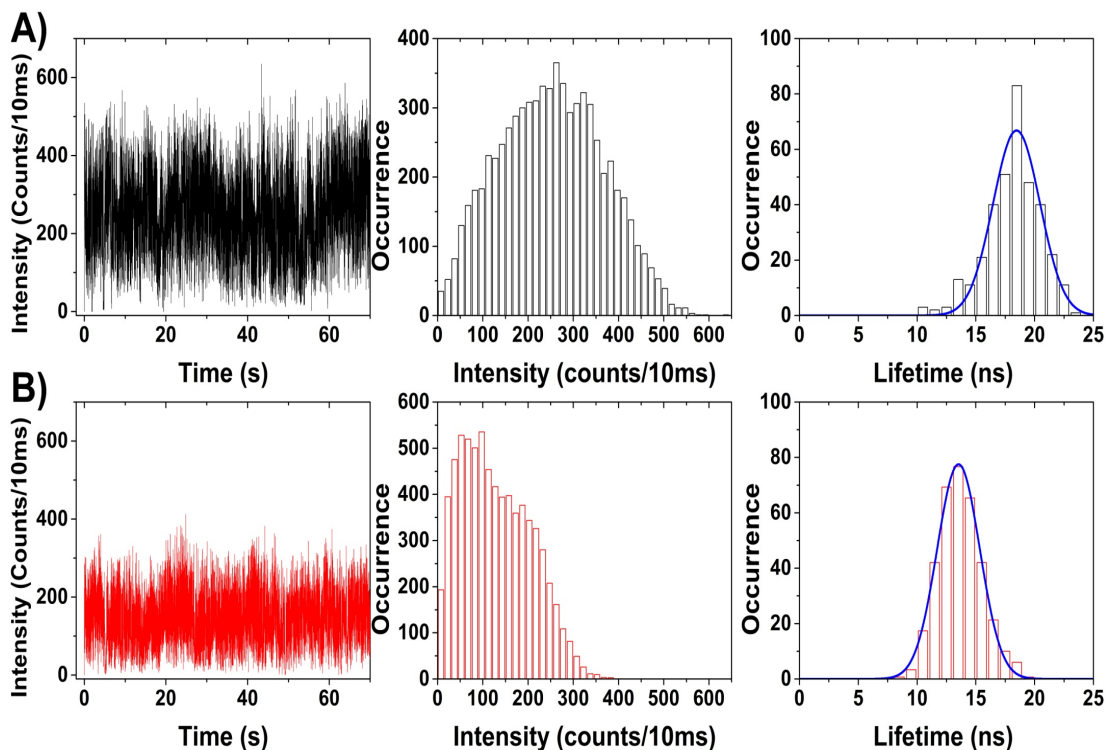


**Figure 11. (A) Free DIR (B) Quenched DIR; left to right are the fluorescence intensity trajectories, intensity histograms and lifetime histograms respectively at one location on the DIR using a TiO<sub>2</sub> NP modified AFM tip.**

To see whether this effect has any distance dependence, the tip was moved to a different location on the DIR, and same measurements were carried out again. Mean intensities and mean lifetimes were then plotted vs. position of the tip along the DIR, and the quenching rate was calculated, as can be clearly seen in Figure 12. We found that the quenching is uniform across the length of the DIR, when in contact with the modified tip. We attribute this quenching to occurring by a thermally activated electron hopping process (discussed earlier).

Similar measurements were carried out with a commercial Pt AFM tip and again uniform quenching (Figure 13a) was observed. Figure 13b shows negligible difference in the maximum and minimum quenching rates ( $K_{\max}$  and  $K_{\min}$ , respectively), along the

lengths of 16 different DIRs, again suggesting that quenching is uniform throughout the length of the DIR.

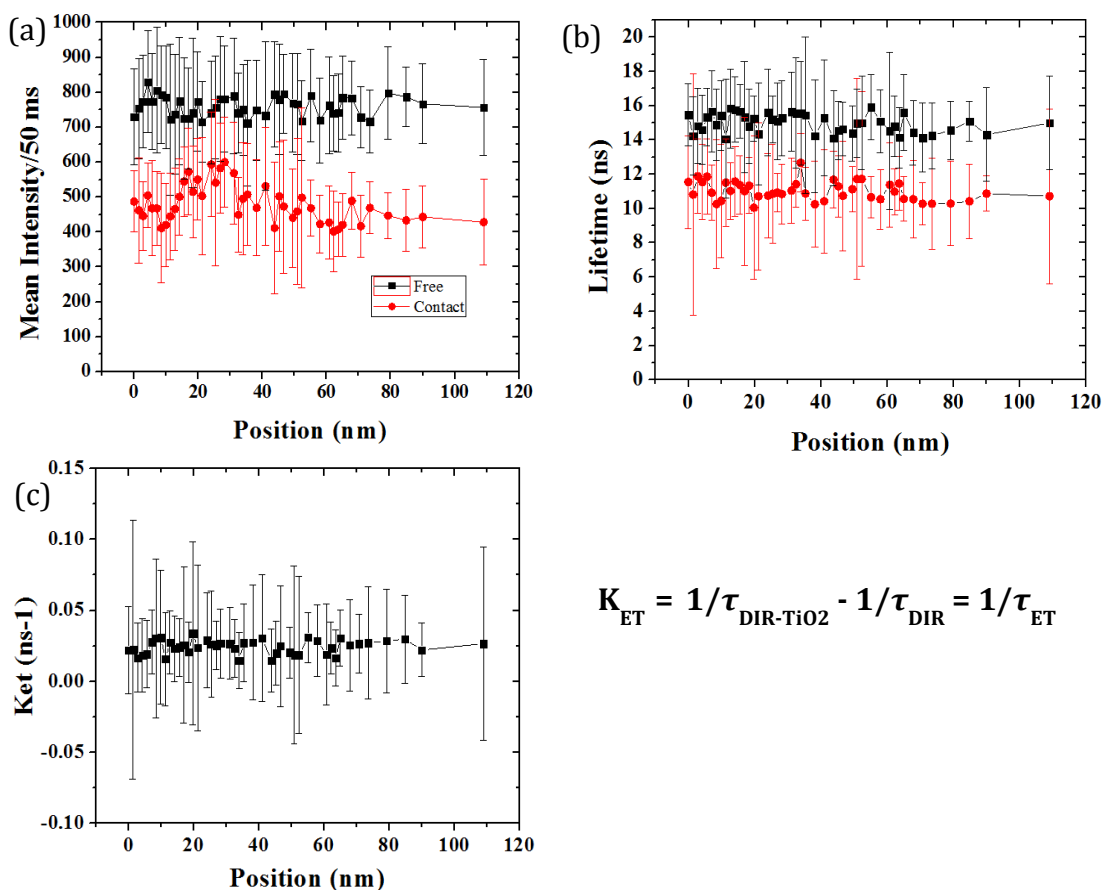


**Figure 12. (a) Mean intensity and (b) mean lifetime of the free DIR (black) and quenched DIR (red) respectively, (c) shows the quenching rates at different locations of the TiO<sub>2</sub> NP AFM tip on the DIR.**

Control experiments with regular or unmodified Si tips were also done (Figure 14), and no quenching was observed (very less/no changes in fluorescence intensities and lifetimes), thus implying that in contact mode, no energy transfer can be seen, since electron transfer cannot take place to these regular tips.

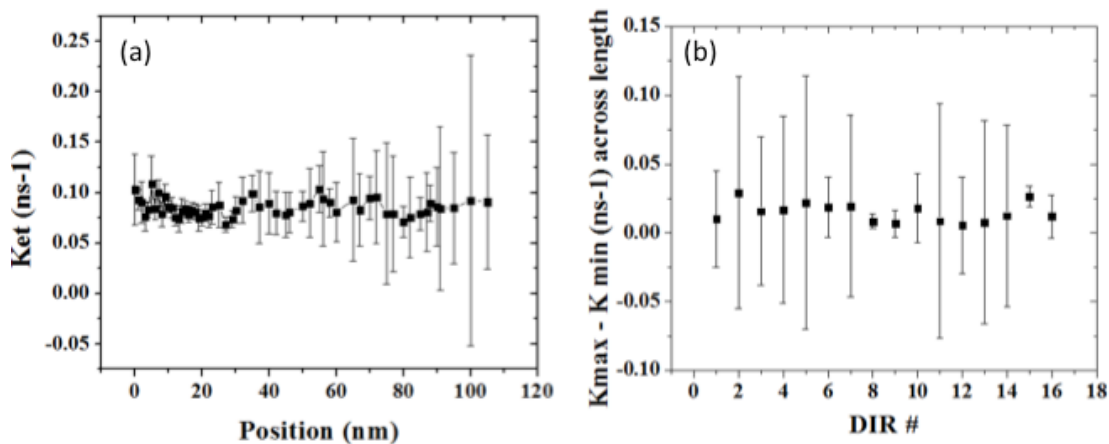


Figure 13. (a) Quenching rate using Pt AFM tip at different locations along a single DIR. (b) Similar experiments were done on a total of 16 single DIRs, and difference in quenching rates was found along the length of the DIR.

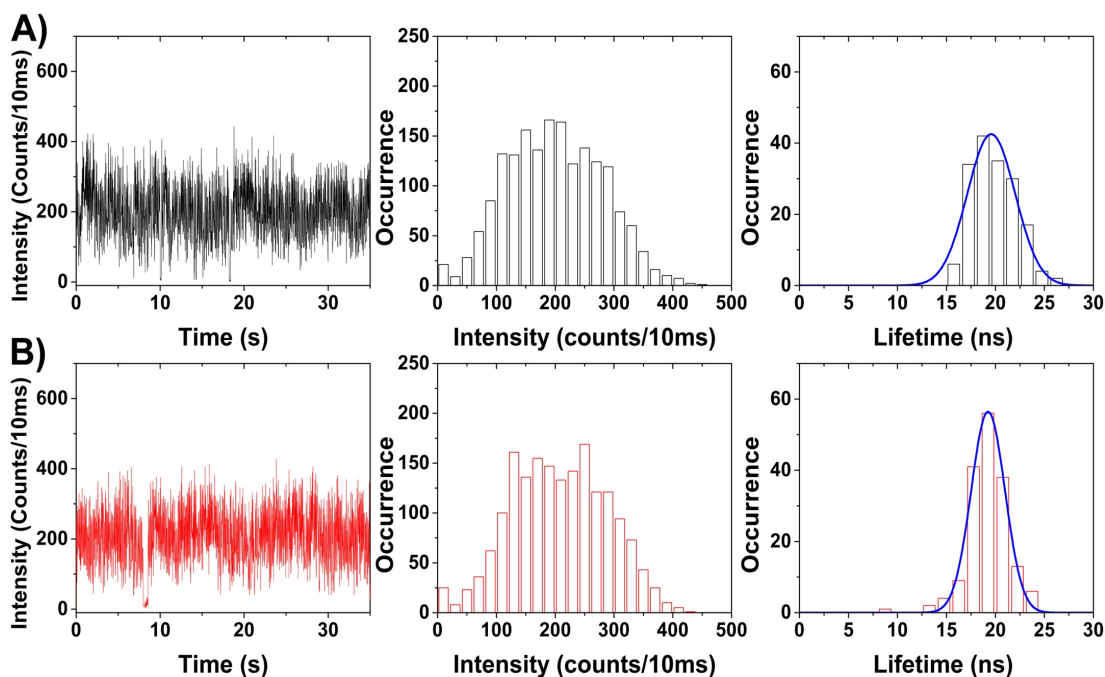


Figure 14. No quenching can be observed with regular Si AFM tip. (A) Free DIR (B) DIR in contact with Si AFM tip; left to right are the fluorescence intensity

trajectories, intensity histograms and lifetime histograms respectively at one location on the DIR using a Si AFM tip.

Cross-section dependent quenching experiment was done to see whether the quenching can occur when the modified tip is far away from the DIR (Figure 15). For this study, the tip was moved along the cross-section of the DIR shown by the blue line in Figure 15a. Quenching rates were calculated at different positions along this line as shown in Figure 15b.

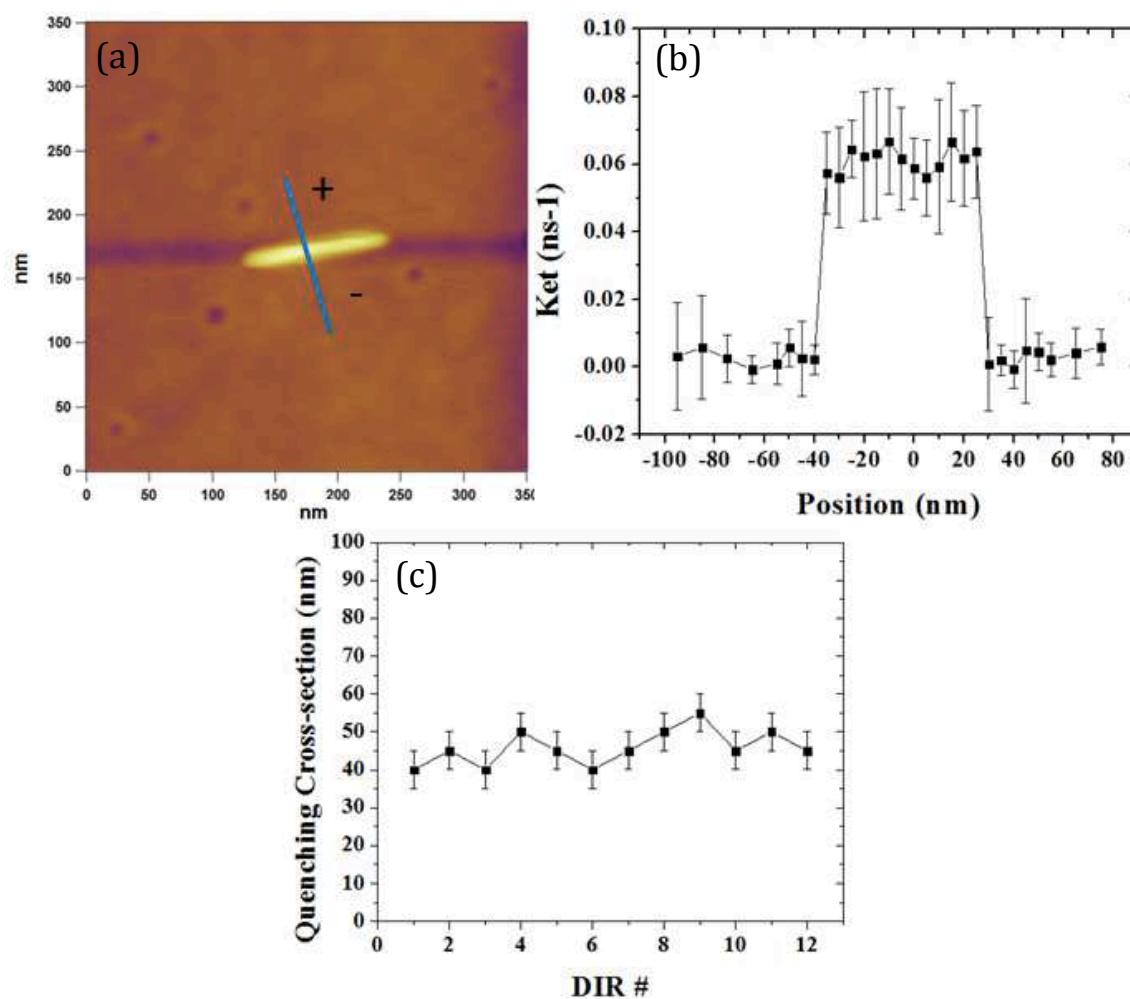


Figure 15. Cross-section dependent quenching experiment: (a) The modified AFM tip was moved along the blue, (b) Fluorescence Quenching rates along the blue line,

### (c) Quenching cross-section (FWHM) from 12 different DIRs

Clearly, quenching only occurred only for a distance of  $\sim 45\text{-}50$  nm (FWHM from Figure 15b), this distance is similar to the radius of the Pt AFM tips. These studies showed that quenching through ET is clearly dependent on the tip-material, radius and geometry. This also suggest energy transfer is not taking place, as when the tip is moved far away from the DIR along the blue line, no quenching was observed. Figure 15c shows the cross-section dependent study on 12 different single DIRs and the results are consistent with each other.

Vertical tip-DIR separation (Figure 16) showed that the quenching can occur only when the tip is in contact with the DIR. In contact mode, the tip is in full contact with the surface as the sample is scanned, while maintaining a user defined deflection voltage (i.e., force) to keep a positive deflection on the cantilever (bows towards surface).

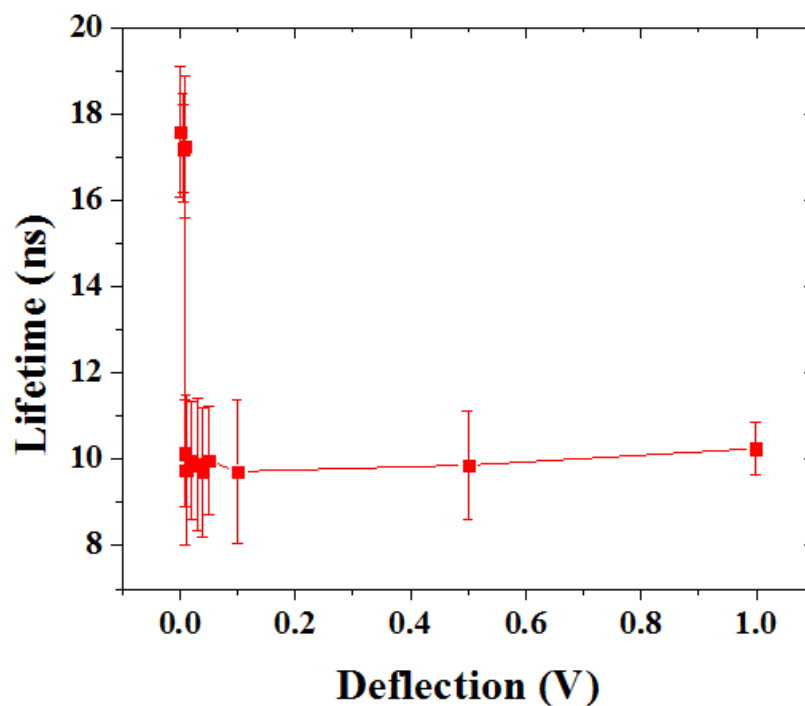


Figure 16. Vertical tip-DIR separation study

By increasing the deflection voltage of the AFM tip, we can control the vertical distance between the tip and the DIR. No quenching was observed, when the tip was not in contact, but once the contact is established ET can take place. Increasing the deflection voltages beyond this, did not result in any change in the quenching rates (Figure 16). Even in this case, energy transfer can be ruled out to be taking place.

One possible explanation for not seeing the quenching exclusively at the core location, as observed by Banin and co-workers,<sup>68</sup> or having uniform quenching throughout the length of the DIR in our results, can be the amount of ligands passivating the DIR surface. They attribute the quenching in fluorescence occurring via a energy transfer channel, and predominantly occurring at the core location. In our case, no energy transfer was found to take place, as shown in the cross-section, vertical tip-DIR separation, and control experiments with Si AFM tip experiments. In our case it is highly possible, that the single DIRs are surrounded by relatively lesser ligands, and the electrons can reach the TiO<sub>2</sub>/Pt AFM tip via a thermally activated electron hopping process, and show uniform quenching along the length of the DIR. The presence of excess ligands in the samples used by Banin and co-workers, inhibit this process and only energy transfer is observed.

### Summary and Future Outlook:

To conclude, the interfacial ET from single DIR to TiO<sub>2</sub> or Pt was investigated using single molecule fluorescence spectroscopy. Single molecule fluorescence studies reveal static and dynamic heterogeneities that remain hidden in ensemble measurements and provide detailed insight into the electron transfer process. Fluorescence quenching in single CdSe/CdS DIR was shown by using modified AFM tips (TiO<sub>2</sub> and Pt). The quenching rate was uniform throughout the length of the nanorod, suggesting that the tip-DIR interaction is giving rise to this effect and does not depend on the core location, unlike previously reported results in the literature.<sup>68</sup> This ET to TiO<sub>2</sub> or Pt has to be the rate-determining step, which dominates over ionization, diffusion and recombination mechanisms. The quenching was attributed to occur via a thermally activated electron hopping process. Further theoretical studies are underway in our group to prove this is indeed the case.

Vertical distance dependence study, showed that this quenching occurs when the tip is in contact with the DIR. Cross-section dependence further showed that quenching depends on the tip radius, material and geometry. Although this quenching effect was shown to be reproducible in different DIRs, but the exact understanding of the quenching mechanism by electron transfer needs to be further explored.

Fluorescence quenching using a modified AFM tip can also be used in visualizing imaging exciton diffusion within a nanocrystal using wide-field imaging techniques. It has been shown that excitons can diffuse within a perovskite nanocrystal.<sup>95</sup> Fluorescence quenching using a modified AFM tip to study this diffusion process can give us further insights to calculate the diffusion length, charge carrier lifetimes and other interesting

properties of these nanocrystals.

#### References:

- (1) Lakowicz, J. R. *Principles of Fluorescence Spectroscopy*; Springer, 2006.
- (2) Dahan, M.; Levi S Fau - Luccardini, C.; Luccardini C Fau - Rostaing, P.; Rostaing P Fau - Riveau, B.; Riveau B Fau - Triller, A.; Triller, A. *Science* 2003, *302*, 442.
- (3) Andrews, N. L.; Lidke, K. A.; Pfeiffer, J. R.; Burns, A. R.; Wilson, B. S.; Oliver, J. M.; Lidke, D. S. *Nat Cell Biol* 2008, *10*, 955.
- (4) Ballou, B.; Lagerholm Bc Fau - Ernst, L. A.; Ernst La Fau - Bruchez, M. P.; Bruchez Mp Fau - Waggoner, A. S.; Waggoner, A. S. *Bioconjugate Chem* 2004, *15*.
- (5) Pinaud, F.; Michalet X Fau - Bentolila, L. A.; Bentolila La Fau - Tsay, J. M.; Tsay Jm Fau - Doose, S.; Doose S Fau - Li, J. J.; Li Jj Fau - Iyer, G.; Iyer G Fau - Weiss, S.; Weiss, S.
- (6) Bruchez, M.; Moronne, M.; Gin, P.; Weiss, S.; Alivisatos, A. P. *Science* 1998, *281*, 2013.
- (7) Colvin, V. L.; Schlamp, M. C.; Alivisatos, A. P. *Nature* 1994, *370*, 354.
- (8) Anikeeva, P. O.; Halpert, J. E.; Bawendi, M. G.; Bulović, V. *Nano Letters* 2007, *7*, 2196.
- (9) Caruge, J. M.; Halpert, J. E.; Wood, V.; Bulovic, V.; Bawendi, M. G. *Nat Photon* 2008, *2*, 247.
- (10) Huynh, W. U.; Dittmer, J. J.; Alivisatos, A. P. *Science* 2002, *295*, 2425.
- (11) Biju, V.; Micic, M.; Hu, D.; Lu, H. P. *Journal of the American Chemical Society* 2004, *126*, 9374.
- (12) Issac, A.; Jin, S.; Lian, T. *Journal of the American Chemical Society* 2008, *130*, 11280.
- (13) Jin, S.; Song, N.; Lian, T. *ACS Nano* 2010, *4*, 1545.
- (14) Song, N.; Zhu, H.; Jin, S.; Zhan, W.; Lian, T. *ACS Nano* 2010, *5*, 613.
- (15) Jin, S.; Lian, T. *Nano Letters* 2009, *9*, 2448.
- (16) Nirmal, M.; Dabbousi, B. O.; Bawendi, M. G.; Macklin, J. J.; Trautman, J. K.; Harris, T. D.; Brus, L. E. *Nature* 1996, *383*, 802.
- (17) Empedocles, S.; Norris, D.; Bawendi, M. *Physical Review Letters* 1996, *77*, 3873.
- (18) Wu, X.; Liu, H.; Liu, J.; Haley, K. N.; Treadway, J. A.; Larson, J. P.; Ge, N.; Peale, F.; Bruchez, M. P. *Nat Biotech* 2003, *21*, 41.
- (19) Medintz, I. L.; Uyeda, H. T.; Goldman, E. R.; Mattoussi, H. *Nat Mater* 2005, *4*, 435.
- (20) Freeman, R.; Willner, I. *Chemical Society Reviews* 2012, *41*, 4067.
- (21) Empedocles, S. A.; Bawendi, M. G. *The Journal of Physical Chemistry B* 1999, *103*, 1826.
- (22) Dabbousi, B. O.; Rodriguez-Viejo, J.; Mikulec, F. V.; Heine, J. R.; Mattoussi, H.; Ober, R.; Jensen, K. F.; Bawendi, M. G. *The Journal of Physical Chemistry B* 1997, *101*, 9463.

- (23) Hines, M. A.; Guyot-Sionnest, P. *The Journal of Physical Chemistry* 1996, *100*, 468.
- (24) Mahler, B.; Spinicelli, P.; Buil, S.; Quelin, X.; Hermier, J.-P.; Dubertret, B. *Nat Mater* 2008, *7*, 659.
- (25) Galland, C.; Brovelli, S.; Bae, W. K.; Padilha, L. A.; Meinardi, F.; Klimov, V. I. *Nano Letters* 2013, *13*, 321.
- (26) Talapin, D. V.; Koeppel, R.; Götzinger, S.; Kornowski, A.; Lupton, J. M.; Rogach, A. L.; Benson, O.; Feldmann, J.; Weller, H. *Nano Letters* 2003, *3*, 1677.
- (27) Carbone, L.; Nobile, C.; De Giorgi, M.; Sala, F. D.; Morello, G.; Pompa, P.; Hytch, M.; Snoeck, E.; Fiore, A.; Franchini, I. R.; Nadasan, M.; Silvestre, A. F.; Chiodo, L.; Kudera, S.; Cingolani, R.; Krahne, R.; Manna, L. *Nano Letters* 2007, *7*, 2942.
- (28) Efros, A. L.; Rosen, M.; Kuno, M.; Nirmal, M.; Norris, D. J.; Bawendi, M. *Physical Review B* 1996, *54*, 4843.
- (29) Klimov, V. I. *Semiconductor and Metal Nanocrystals: Synthesis and Electronic and Optical Properties*; CRC Press, 2003.
- (30) Woggon, U.; Gaponenko, S.; Langbein, W.; Uhrig, A.; Klingshirn, C. *Physical Review B* 1993, *47*, 3684.
- (31) Kamat, P. V. *The Journal of Physical Chemistry Letters* 2012, *3*, 663.
- (32) Lounis, B.; Bechtel, H. A.; Gerion, D.; Alivisatos, P.; Moerner, W. E. *Chemical Physics Letters* 2000, *329*, 399.
- (33) Michler, P.; Imamoglu, A.; Mason, M. D.; Carson, P. J.; Strouse, G. F.; Buratto, S. K. *Nature* 2000, *406*, 968.
- (34) Fisher, B.; Caruge, J. M.; Zehnder, D.; Bawendi, M. *Physical Review Letters* 2005, *94*, 087403.
- (35) Zhu, H.; Song, N.; Lian, T. *Journal of the American Chemical Society* 2011, *133*, 8762.
- (36) Zhu, H.; Song, N.; Rodríguez-Córdoba, W.; Lian, T. *Journal of the American Chemical Society* 2012, *134*, 4250.
- (37) Zhu, H.; Lian, T. *Energy & Environmental Science* 2012, *5*, 9406.
- (38) Reiss, P.; Protiere, M.; Li, L. *Small* 2009, *5*, 154.
- (39) Kim, S.; Fisher, B.; Eisler, H.-J.; Bawendi, M. *Journal of the American Chemical Society* 2003, *125*, 11466.
- (40) Ivanov, S. A.; Piryatinski, A.; Nanda, J.; Tretiak, S.; Zavadil, K. R.; Wallace, W. O.; Werder, D.; Klimov, V. I. *Journal of the American Chemical Society* 2007, *129*, 11708.
- (41) Kim, S.; Lim, Y. T.; Soltesz, E. G.; De Grand, A. M.; Lee, J.; Nakayama, A.; Parker, J. A.; Mihaljevic, T.; Laurence, R. G.; Dor, D. M.; Cohn, L. H.; Bawendi, M. G.; Frangioni, J. V. *Nat Biotech* 2004, *22*, 93.
- (42) Nanda, J.; Ivanov, S. A.; Achermann, M.; Bezel, I.; Piryatinski, A.; Klimov, V. I. *The Journal of Physical Chemistry C* 2007, *111*, 15382.
- (43) Sitt, A.; Sala, F. D.; Menagen, G.; Banin, U. *Nano Letters* 2009, *9*, 3470.
- (44) García-Santamaría, F.; Chen, Y.; Vela, J.; Schaller, R. D.; Hollingsworth, J. A.; Klimov, V. I. *Nano Letters* 2009, *9*, 3482.
- (45) Eshet, H.; Grünwald, M.; Rabani, E. *Nano Letters* 2013, *13*, 5880.

- (46) Morello, G.; Della Sala, F.; Carbone, L.; Manna, L.; Maruccio, G.; Cingolani, R.; De Giorgi, M. *Physical Review B* 2008, 78, 195313.
- (47) Borys, N. J.; Walter, M. J.; Huang, J.; Talapin, D. V.; Lupton, J. M. *Science* 2010, 330, 1371.
- (48) Rabouw, F. T.; Lunnemann, P.; van Dijk-Moes, R. J. A.; Frimmer, M.; Pietra, F.; Koenderink, A. F.; Vanmaekelbergh, D. *Nano Letters* 2013, 13, 4884.
- (49) Mokari, T.; Rothenberg, E.; Popov, I.; Costi, R.; Banin, U. *Science* 2004, 304, 1787.
- (50) Costi, R.; Saunders, A. E.; Elmaleh, E.; Salant, A.; Banin, U. *Nano Letters* 2008, 8, 637.
- (51) Wu, K.; Chen, J.; McBride, J. R.; Lian, T. *Science* 2015, 349, 632.
- (52) Wu, K.; Rodríguez-Córdoba, W. E.; Yang, Y.; Lian, T. *Nano Letters* 2013, 13, 5255.
- (53) Chen, X.; Shen, S.; Guo, L.; Mao, S. S. *Chemical Reviews* 2010, 110, 6503.
- (54) Wu, K.; Zhu, H.; Liu, Z.; Rodríguez-Córdoba, W.; Lian, T. *Journal of the American Chemical Society* 2012, 134, 10337.
- (55) Acharya, K. P.; Khnayzer, R. S.; O'Connor, T.; Diederich, G.; Kirsanova, M.; Klinkova, A.; Roth, D.; Kinder, E.; Imboden, M.; Zamkov, M. *Nano Letters* 2011, 11, 2919.
- (56) Amirav, L.; Alivisatos, A. P. *The Journal of Physical Chemistry Letters* 2010, 1, 1051.
- (57) Wu, K.; Chen, Z.; Lv, H.; Zhu, H.; Hill, C. L.; Lian, T. *Journal of the American Chemical Society* 2014, 136, 7708.
- (58) Nakibli, Y.; Kalisman, P.; Amirav, L. *The Journal of Physical Chemistry Letters* 2015, 6, 2265.
- (59) Razgoniaeva, N.; Moroz, P.; Lambright, S.; Zamkov, M. *The Journal of Physical Chemistry Letters* 2015, 6, 4352.
- (60) Wu, K.; Zhu, H.; Lian, T. *Accounts of Chemical Research* 2015, 48, 851.
- (61) Ebenstein, Y.; Yoskovitz, E.; Costi, R.; Aharoni, A.; Banin, U. *The Journal of Physical Chemistry A* 2006, 110, 8297.
- (62) Kühn, S.; Sandoghdar, V. *Applied Physics B* 2006, 84, 211.
- (63) Lupo, M. G.; Della Sala, F.; Carbone, L.; Zavelani-Rossi, M.; Fiore, A.; Lürer, L.; Polli, D.; Cingolani, R.; Manna, L.; Lanzani, G. *Nano Letters* 2008, 8, 4582.
- (64) Zhu, H.; Song, N.; Lian, T. *Journal of the American Chemical Society* 2010, 132, 15038.
- (65) Davis, W. B.; Wasielewski, M. R.; Ratner, M. A.; Mujica, V.; Nitzan, A. *The Journal of Physical Chemistry A* 1997, 101, 6158.
- (66) Segal, D.; Nitzan, A.; Davis, W. B.; Wasielewski, M. R.; Ratner, M. A. *The Journal of Physical Chemistry B* 2000, 104, 3817.
- (67) Segal, D.; Nitzan, A.; Ratner, M.; Davis, W. B. *The Journal of Physical Chemistry B* 2000, 104, 2790.
- (68) Yoskovitz, E.; Menagen, G.; Sitt, A.; Lachman, E.; Banin, U. *Nano Letters* 2010, 10, 3068.

- (69) Dorfs, D.; Salant, A.; Popov, I.; Banin, U. *Small* 2008, 4, 1319.
- (70) Müller, J.; Lupton, J. M.; Lagoudakis, P. G.; Schindler, F.; Koeppe, R.; Rogach, A. L.; Feldmann, J.; Talapin, D. V.; Weller, H. *Nano Letters* 2005, 5, 2044.
- (71) She, C.; Guo, J.; Lian, T. *The Journal of Physical Chemistry B* 2007, 111, 6903.
- (72) Chung, I.; Bawendi, M. *Physical Review B* 2004, 70, 165304.
- (73) Zhang, K.; Chang, H.; Fu, A.; Alivisatos, A. P.; Yang, H. *Nano Letters* 2006, 6, 843.
- (74) Mathew, S.; Yella, A.; Gao, P.; Humphry-Baker, R.; CurchodBasile, F. E.; Ashari-Astani, N.; Tavernelli, I.; Rothlisberger, U.; NazeeruddinMd, K.; Grätzel, M. *Nat Chem* 2014, 6, 242.
- (75) Johansson, P. G.; Kopecky, A.; Galoppini, E.; Meyer, G. J. *Journal of the American Chemical Society* 2013, 135, 8331.
- (76) Cordones, A. A.; Leone, S. R. *Chemical Society Reviews* 2013, 42, 3209.
- (77) Ye, S.; Kathiravan, A.; Hayashi, H.; Tong, Y.; Infahsaeng, Y.; Chabera, P.; Pascher, T.; Yartsev, A. P.; Isoda, S.; Imahori, H.; Sundström, V. *The Journal of Physical Chemistry C* 2013, 117, 6066.
- (78) Farnum, B. H.; Morseth, Z. A.; Lapidés, A. M.; Rieth, A. J.; Hoertz, P. G.; Brennaman, M. K.; Papanikolas, J. M.; Meyer, T. J. *Journal of the American Chemical Society* 2014, 136, 2208.
- (79) Anderson, N. A.; Lian, T. *Annual Review of Physical Chemistry* 2004, 56, 491.
- (80) Watson, D. F.; Meyer, G. J. *Annual Review of Physical Chemistry* 2004, 56, 119.
- (81) Jin, S.; Hsiang, J.-C.; Zhu, H.; Song, N.; Dickson, R. M.; Lian, T. *Chemical Science* 2010, 1, 519.
- (82) Yoskovitz, E.; Hadar, I.; Sitt, A.; Lieberman, I.; Banin, U. *The Journal of Physical Chemistry C* 2011, 115, 15834.
- (83) Frantsuzov, P. A.; Volkán-Kacsó, S.; Jankó, B. *Nano Letters* 2013, 13, 402.
- (84) BradacC; GaebelT; NaidooN; Sellars, M. J.; TwamleyJ; Brown, L. J.; Barnard, A. S.; PlakhotnikT; Zvyagin, A. V.; Rabeau, J. R. *Nat Nano* 2010, 5, 345.
- (85) Bout, D. A. V.; Yip, W.-T.; Hu, D.; Fu, D.-K.; Swager, T. M.; Barbara, P. F. *Science* 1997, 277, 1074.
- (86) Moerner, W. E.; Orrit, M. *Science* 1999, 283, 1670.
- (87) Shimizu, K.; Neuhauser, R.; Leatherdale, C.; Empedocles, S.; Woo, W.; Bawendi, M. *Physical Review B* 2001, 63, 205316.
- (88) Efros, A. L.; Rosen, M. *Physical Review Letters* 1997, 78, 1110.
- (89) Krauss, T. D.; O'Brien, S.; Brus, L. E. *The Journal of Physical Chemistry B* 2001, 105, 1725.
- (90) Fisher, B. R.; Eisler, H.-J.; Stott, N. E.; Bawendi, M. G. *The Journal of Physical Chemistry B* 2004, 108, 143.
- (91) Chung, I.; Bawendi, M. G. *Physical Review B* 2004, 70, 165304.
- (92) Kuno, M.; Fromm, D. P.; Gallagher, A.; Nesbitt, D. J.; Micic, O. I.; Nozik, A. J. *Nano Letters* 2001, 1, 557.

- (93) Peterson, J. J.; Nesbitt, D. J. *Nano Letters* 2009, 9, 338.
- (94) Galland, C.; Ghosh, Y.; Steinbruck, A.; Sykora, M.; Hollingsworth, J. A.; Klimov, V. I.; Htoon, H. *Nature* 2011, 479, 203.
- (95) Tian, W.; Zhao, C.; Leng, J.; Cui, R.; Jin, S. *Journal of the American Chemical Society* 2015, 137, 12458.
- (96) Anderson, N. A.; Ai, X.; Lian, T. *The Journal of Physical Chemistry B* 2003, 107, 14414.
- (97) Palomares, E.; Clifford, J. N.; Haque, S. A.; Lutz, T.; Durrant, J. R. *Journal of the American Chemical Society* 2003, 125, 475.
- (98) Ghosh, H. N.; Asbury, J. B.; Lian, T. *The Journal of Physical Chemistry B* 1998, 102, 6482.
- (99) Dong, L.; Sugunan A Fau - Hu, J.; Hu J Fau - Zhou, S.; Zhou S Fau - Li, S.; Li S Fau - Popov, S.; Popov S Fau - Toprak, M. S.; Toprak Ms Fau - Friberg, A. T.; Friberg At Fau - Muhammed, M.; Muhammed, M.
- (100) Wang, S.; Querner, C.; Emmons, T.; Drndic, M.; Crouch, C. H. *The Journal of Physical Chemistry B* 2006, 110, 23221.
- (101) Tang, J.; Marcus, R. A. *Physical Review Letters* 2005, 95, 107401.